Title
SHORT RANGE ORDER IN Ni-Mo, Au-Cr, Au-V AND Au-Mn ALLOYS

Author
Das, S.K.

Publication Date
1972-12-01

Submitted to Acta Metallurgica

LBL-441 Rev.
Preprint

SHORT RANGE ORDER IN Ni-Mo, Au-Cr, Au-V AND Au-Mn ALLOYS

S. K. Das, P. R. Okamoto, P. M. J. Fisher, and G. Thomas

December 1972

Prepared for the U. S. Atomic Energy Commission
under Contract W-7405-ENG-48

LBL-441 Rev.

DISCLAIMER

SHORT RANGE ORDER IN Ni-Mo, Au-Cr, Au-V and Au-Mn ALLOYS

S. K. Das,[1] P. R. Okamoto,[1] P. M. J. Fisher[2] and G. Thomas

Inorganic Materials Research Division, Lawrence Berkeley Laboratory and Department of Materials Science and Engineering, College of Engineering; University of California, Berkeley, California 94720

ABSTRACT

The nature of short range order (sro) has been investigated in the series of alloys Ni_4Mo, Ni_3Mo, Au_3Cr, Au_4Cr, Au_3Mn and Au_4V, which exhibit different long range ordered (lro) structures, by transmission electron microscopy and diffraction. The examination of the sro state, at temperatures above the critical temperatures (T_c) for the order-disorder transformations and also in the samples that were quenched from above T_c, showed diffuse scattering peaks centered near $\{1\frac{1}{2}0\}$ positions in the fcc reciprocal lattice, whose shape changed from one system to another. Evidence for diffuse scattering near superlattice positions corresponding to the D1a structure was obtained in the sro state of Au-Cr, Au-V and Ni-Mo alloys. Additional diffuse scattering was observed near Ni_2Mo positions in the Ni-Mo alloys. The diffraction patterns of Au_3Mn above T_c showed evidence for diffuse scattering near the superlattice positions corresponding to the Watanabe type two-dimensional long period superstructure.

---

1. Now at Argonne National Laboratory, Argonne, Illinois
2. Now at Monash University, Melbourne, Australia

Inclusion of pairwise interaction parameters up to third nearest neighbors in the high temperature statistical mechanical model of Clapp and Moss partially accounts for the shapes of $\{1\frac{1}{2}0\}$ sro spots found in Ni-Mo and Au-Mn alloys, but not in Au-Cr and Au-V alloys. The shapes of the diffuse sro scattering in the latter alloys, however, can be interpreted in terms of a distribution of various types of imperfectly ordered microdomains existing above the critical temperature. For a particular stoichiometry, the most frequently occurring microdomain may or may not correspond to the equilibrium long range ordered (lro) structure of the alloy.

1. INTRODUCTION

A solid solution having short range order (sro) usually exhibits diffuse maxima in the diffraction patterns. The high temperature statistical mechanical approximation of Clapp and Moss[1,2] (C-M) appears to be capable of explaining the diffuse scattering distribution obtained at sufficiently high temperatures where the degree of sro is very small. However, as the critical ordering temperature (T_c) is approached from temperatures above T_c, non-linear effects come into play which may eventually invalidate the C-M model near T_c. In this case the concept of microdomains, often used to interpret the diffuse scattering distributions, becomes very helpful.

In the classical microdomain model the diffuse sro maxima are interpreted to arise from small particle broadening effects, of the superlattice reflections arising from a contiguous distribution of

very small ordered domains. This model therefore imples that the positions of the sro maxima in reciprocal space should always coincide with those of the superlattice reflections. However, certain systems such as Ni_4Mo[3], Ni_4W[4], Au_3Cr[5] and several Ti-O alloys,[6] have been found to exhibit diffuse sro maxima at positions other than at the superlattice positions. The long range ordered (lro) states of the first three alloys have the body centered tetragonal (Dla) structure. Above T_c these alloys are disordered fcc and show sro diffuse maxima at all equivalent $\{1\frac{1}{2}0\}$ positions of the fcc reciprocal lattice, which are not Dla superlattice positions. Thus this classical microdomain model fails to explain the position of sro maxima in these systems. On the other hand the C-M model successfully predicts both the position and the shape of the $\{1\frac{1}{2}0\}$ maxima in Ni_4Mo. This suggests that classical microdomain model is not a valid description of sro at least in Ni_4Mo. Recently Okamoto and Thomas[7,8] have argued that the microdomain concept is not necessarily incompatible with the C-M model in Ni_4Mo. The presence of microdomains was inferred from the diffraction evidence that samples of Ni_4Mo quenched from above T_c showed weak scattering near Dla positions co-existing with much stronger $\{1\frac{1}{2}0\}$ peaks. They concluded that the presence of imperfectly ordered microdomains based on the Dla and DO_{22} structures could account for the observed diffraction effects.

The implication that the sro state may consist of a distribution of ordered microdomains possessing different but closely related structures is supported by the recent theoretical work of Clapp.[9]

He has used a probability variation method (PVM)[10] to determine the complete frequency distribution of nearest neighbor configurations for a number of cubic alloys from their experimentally determined sro parameters. His calculations show that the most enhanced configuration relative to the random state often corresponded to the perfectly ordered state, although its volume fraction may be very small. There are also departures from this simple expectation, although it is not clear how many cases (if any) result from data limitation. His calculations on Au_3Cu ($L1_2$ structure) show a rather surprising result that the most enhanced clusters are the $L1_0$ (CuAu) type and the fourth most enhanced clusters are Cu_3Au type. This implies that the structure of the clusters present in the sro state in a stoichiometric alloy may not always correspond to the equilibrium lro structure observed at that stoichiometric composition. Moreover, there may be present various types of clusters corresponding to different superstructures.

In view of these results, a systematic study of the sro state in a number of alloys such as Ni_4Mo, Ni_3Mo, Au_3Cr, Au_4Cr, Au_3Mn and Au_4V has been carried out in the present work, in order to obtain evidence of multiple microdomain configurations in these systems. The choice of these alloys stems from the fact that all of them do not have the same lro structure, yet they all exhibit sro diffuse maxima at the $\{1\frac{1}{2}0\}$ positions. An attempt has been made to explain the diffuse scattering results from these systems with the help of the C-M model. This model, although very good in explaining most of the gross features of the diffuse scattering was unable to account for all of the details.

The presence of multiple microdomain configurations, however, qualitatively accounts for all of the observed features.

2. EXPERIMENTAL PROCEDURE

Bulk alloys of Au_3Cr, Ni_4Mo, Ni_3Mo and Au_4V were prepared by melting together required proportions of the individual components in an arc furnace, back filled with argon. The purity of all the starting materials was 99.99% except for vanadium which was 99.9% pure. The alloys were melted several times in the furnace in order to obtain homogeneity. The ingots were encapsulated in quartz tubes in vacuum and were homogenized at suitable temperatures. The compositions of the bulk alloys and their corresponding homogenization temperatures are shown in Table 1. The ingots were cold rolled to 6 mil strips with intermediate anneals. The foils were then finally homogenized in an inert atmosphere and quenched directly into iced brine from their homogenization temperature.

The thin foils of Ni-Mo alloys for transmission electron microscopy were prepared by jet polishing in an electrolyte containing two parts of sulphuric acid and one part water. The thin foils of Au alloys were relatively difficult to prepare and the window method was used

TABLE 1. Composition of the Bulk Alloys

Alloy	Atomic % Solute	Homogenization Temp (°C)
Ni_4Mo	Mo - 19.7	1200
Ni_3Mo	Mo - 25.1	1270
Au_3Cr	Cr - 23.5	900
Au_4V	V - 19.1	900

with an electrolyte containing 88 gms. of chromic oxide, 465cc acetic acid, 25cc water.

300-600 Å single crystal thin films of Au_3Cr were prepared by vacuum deposition of the bulk alloy onto freshly cleaved ⟨100⟩ faces of NaCl substrates held at 450°C. The substrate was degassed at 500°C for 1/2 hour prior to deposition. This gave fairly large single crystal thin films of ⟨100⟩ orientation. The samples were homogenized for 2 hours at 400°C and mounted on platinum grids. Further annealing was done inside the microscope. The thin films of Au_4Cr were prepared in a similar manner by melting together required amounts of Au with the bulk Au_3Cr on the filament to form the alloy Au_4Cr and then evaporating on to the heated rock salt. The evaporated thin films of Au_3Mn were obtained from Dr. Lee Tanner of Kennecott Copper Corporation and were similar to those employed in his studies.[5]

All the microscopy was done on a Siemens Elmiskop IA operated at 100 kV. A standard Siemens hot stage was used for the high temperature electron diffraction work. The hot stage was calibrated outside the microscope in a vacuum bell jar, similarly to the procedures described elsewhere.[11]

3. RESULTS

The short range order study involved the examination of the electron diffraction patterns of the systems Ni_4Mo, Ni_3Mo, Au_3Cr, Au_4V and Au_3Mn in specimens either quenched from above T_c, or at temperatures above T_c, or both. Because of the large number of systems involved the results obtained on each system will be presented separately. The

important crystallographic features of each of these systems will be pointed out first and then the diffuse scattering results will be described.

3.1 Ni_4Mo: In the &ro state the stoichiometric Ni_4Mo has a body centered tetragonal structure[12] commonly referred to as D1a in the strukturbericht symbol. The crystallographic features of the ordered Ni_4Mo structure are well known,[8,13] and need not be repeated here. One important feature of this structure is that if one considers the stacking of atoms on {420}* planes, every fifth plane contains only Mo atoms and in between planes contain only Ni atoms. Thus, the reciprocal lattice for the ordered structure can be constructed from the fundamental fcc lattice, since the superlattice reflections appear at every $\frac{1}{5}\langle 420 \rangle$ reciprocal lattice vector of the fcc unit cell. The other structure which is important in this study is that of Ni_2Mo which occurs as a metastable phase during the ordering of Ni_3Mo[14] and Ni_4Mo.[15] The atomic arrangement is isomorphous with ordered Pt_2Mo. Like the D1a structure, the Ni_2Mo structure can also be described by the stacking of atoms on either {420} or {220} planes where every third plane contains all Mo and in between all Ni atoms. Thus, the reciprocal lattice of the ordered structure can be constructed from the original fcc lattice, where the superlattice reflections will appear at every $\frac{1}{3}\langle 220 \rangle$ or $\frac{1}{3}\langle 420 \rangle$ reciprocal lattice vectors. This gives rise to six orientation variants of Ni_2Mo corresponding to six

*Unless otherwise specified the indices refer to the fcc lattice.

variants of {220}. Figures 1a and b show the [001] and [$\bar{1}$30] reciprocal lattice sections constructed in the above manner. Here the positions of D1a and Ni_2Mo superlattice spots are shown together with the $\{1\frac{1}{2}0\}$ sro spots. As has been pointed out earlier,[8] the [$\bar{1}$30] orientation is very important for the detection of weak superlattice reflections in the sro state, because this reciprocal lattice section does not contain any $\{1\frac{1}{2}0\}$ sro spots, as can be seen in Fig. 1b. It is to be noted that each $\{1\frac{1}{2}0\}$ sro spot is surrounded by four D1a spots in the form of a tetrahedron with the $\{1\frac{1}{2}0\}$ sro spot at the center and all of these spots are close together. The small open circles in Fig. 1a represent the projection of D1a spots that are located at $\ell = \frac{1}{10}$ th of ⟨002⟩ reciprocal lattice vectors and the open squares in Fig. 1b are the projections of the neighboring $\{1\frac{1}{2}0\}$ sro spots. Keeping these crystallographic features in mind, we can now examine the diffuse scattering results.

Figure 2 shows a [001] diffraction pattern of a freshly quenched Ni_4Mo sample. The diffuse sro maxima can be seen at the $\{1\frac{1}{2}0\}$ positions. In the study of quenched samples of Ni_4Mo, Okamoto and Thomas[8] found weak scattering to be present near the D1a superlattice positions by examining the [$\bar{1}$30] orientation (for the reasons given above). However, if these D1a spots are present, there should be an enhanced scattering of $\{1\frac{1}{2}0\}$ spots towards the D1a positions and as a result the shape of the $\{1\frac{1}{2}0\}$ spots should be somewhat similar to the dotted triangle in Fig. 1a. However, the X-ray diffuse scattering measurements by Spruiell and Stansbury[3] on quenched samples of Ni_4Mo

showed the shape of $\{1\frac{1}{2}0\}$ spots to be quite different from the expected shape. In their diffuse scattering map for quenched Ni_4Mo the outer contours at $(1\frac{1}{2}0)$ were slightly elongated towards the (100) and (210) positions and not like the dotted triangle in Fig. 1(a). In order to resolve this apparent discrepancy isointensity contour maps were drawn on an isodensitracer from a number of diffraction patterns of the quenched samples of Ni_4Mo (e.g. Fig. 2) as is shown in Fig. 3. The original map uses a color code for the relative intensities and Fig. 3 has been redrawn from the original for easy reproduction. The relative intensities are in arbitrary units. On this map the positions of the Dla and the Ni_2Mo superlattice reflections are also marked. It can be seen that the map is very similar to the X-ray map of Spruiell and Stansbury.[3] Here, the diffuse intensities near each of the $\{1\frac{1}{2}0\}$ positions are not exactly the same because the optic axis being at the origin (000), the deviations of each of the $\{1\frac{1}{2}0\}$ spots from the exact Bragg positions are different. However, the distribution of diffuse intensity in Fig. 3 suggests that there may be weak scattering present not only at the Dla positions but also at the superlattice positions corresponding to the Ni_2Mo structure. The observed enhanced scattering of the $(1\frac{1}{2}0)$ spot towards (100) and (210) positions in [001] patterns is most likely to be due to the presence of weak scattering near the Ni_2Mo spots. In order to check this, several other reciprocal lattice sections were examined and Fig. 4 shows a $[\bar{1}30]$ section. The diffuse peaks observed in this pattern are not entirely due to the weak Dla spots as was reported earlier.[8] Careful measurements show

that the centers of these diffuse peaks do not lie exactly at the positions where the Dla spots ought to occur. It can be seen from Fig. 1(b) that the projections of the $\{1\frac{1}{2}0\}$ spots on to the $[\bar{1}30]$ reciprocal lattice section lie very close to those of the Dla spots. The diffuse peaks at A in Fig. 4 are, in fact, elongated towards the projection of $\{1\frac{1}{2}0\}$ spots and have the shape outlined by the dotted lines in Fig. 1(b). Thus, the diffuse Dla peaks are not isolated from the diffuse $\{1\frac{1}{2}0\}$ sro maxima, but merge together with them. The diffuse scattering near 'B' (Fig. 4) is different from that at 'A' and has two wings on either side (marked by arrows) that extend towards the positions of the Ni_2Mo spots [Fig. 1(b)].† This shows that in addition to the diffuse scattering near Dla positions, there must be scattering near Ni_2Mo positions. This has never been reported before. This was further confirmed by examining a [110] section [Fig. 5] which contains only the Ni_2Mo spots and no $\{1\frac{1}{2}0\}$ sro or Dla spots. The arrows in Fig. 5(a) point to the weak peaks that appear at the Ni_2Mo positions as indexed in Fig. 5(b). It must be pointed out that the detection of such weak peaks depends very much on the exposure time. In the underexposed plates these may be missed altogether, and in the present investigation exposure times up to 10 minutes (with a well-defocussed second condensor lens) were necessary to bring out the details. Thus, in the quenched state Ni_4Mo samples exhibit weak scattering near Dla and Ni_2Mo superlattice positions coexisting with much

†These features are rather difficult to reproduce clearly on prints but can be clearly seen on the original plate negatives.

stronger scattering at $\{1\frac{1}{2}0\}$. The scattering at D1a and Ni_2Mo positions are not isolated peaks but emerge from the $\{1\frac{1}{2}0\}$ peaks that lie close to them.

3.2. Ni_3Mo: The equilibrium lro structure of Ni_3Mo has been determined by Saito and Beck[16] to be orthorhombic and isotypic with that of ordered Cu_3Ti. The stoichiometric Ni_3Mo also does not have a true T_c and decomposes peritectoidally at 910°C to α + NiMo and is disordered fcc at high temperatures in the single phase region. On fast quenching from the single phase region the decomposition to Ni-Mo can be suppressed. It has been mentioned[14,17] that the sro state of Ni_3Mo is similar to that of Ni_4Mo, but no detailed studies as to whether any weak superlattice peaks are present or not have yet been reported. During the isothermal annealing the Ni_4Mo and Ni_2Mo phases appear as metastable phases at an early stage and finally the quilibrium Ni_3Mo forms. Thus, it would be interesting to see whether any weak superlattice spots are present in the sro state or not, and if so, of what type.

Figure 6(a) shows a [001] diffraction pattern of Ni_3Mo quenched into iced brine from 1270°C. This pattern is similar to that of Ni_4Mo (Fig. 2). Here the diffuse scattering appears to extend from one $\{1\frac{1}{2}0\}$ position to the neighboring ones in the form of an arc, that passes through the Ni_2Mo position. The $[\bar{1}30]$ diffraction pattern of Ni_3Mo is also similar to that of Ni_4Mo. In all the sections examined no evidence for diffuse scattering near Ni_3Mo positions was obtained e.g. the [110] pattern of Fig. 6(b). Thus the quenched state of Ni_3Mo

is similar to that of Ni_4Mo and there is weak scattering present near the superlattice positions corresponding to the Dla and Ni_2Mo structures, in addition to the $\{1\frac{1}{2}0\}$ peaks. Although it may appear to be surprising that stoichiometric Ni_3Mo does not show Ni_3Mo superlattice spots but only Ni_2Mo and Ni_4Mo superlattice spots, the reason this may be so will be discussed later.

In the as quenched condition it was not possible to obtain any resolvable features in dark field images of the $\{1\frac{1}{2}0\}$ spots, but after slight aging the dark field micrographs did show images which can be interpreted to arise from particles or microdomains. Figure 7(a) is a dark field micrograph of the $\{1\frac{1}{2}0\}$ spot encircled in the diffraction pattern in Fig. 7(b). This image is similar to that obtained by Ruedl et.al.[13] in quenched Ni_4Mo, and shows microdomains of about 30 30-40 Å in diameter, that do not have a well defined shapes, and with diffuse boundaries. In quenched samples of Ni_3Mo, the degree of order within the microdomains may have been too small to provide images of sufficient intensity to give contrast. The microdomains observed by Ruedl et al. in quenched Ni_4Mo were probably resolved because of the slower quenching rate and resulting higher degree of order. Nevertheless, the fact is that microdomains are directly visible in the dark field micrographs of $\{1\frac{1}{2}0\}$ sro spots, when the superlattice reflections are still very diffuse and weak.

Now the question arises as to whether these quenched samples represent the sro state above Tc or not. It is quite possible that some lro might have been induced during the quench itself. To prove

conclusively that these weak superlattice reflections are present in the sro state it is necessary to examine specimens at and near T_c.

In the Ni-Mo system, since the disordering temperatures are rather high, electron diffraction studies near T_c are not very helpful because of the excessive thermal diffuse scattering. Thus, the Au-Cr and Au-Mn systems which have relatively lower T_c were chosen for high temperature electron diffraction studies, to see whether there are any weak superlattice reflections co-existing with $\{1\frac{1}{2}0\}$ maxima.

3.3. Au_3Cr: The equilibrium lro structure of Au_3Cr is not definitely known and the phase diagram of Au-Cr system shows that an ordered phase may be present below 300°C. However, it has been established[5] that in thin films the alloy transforms to the D1a superstructure. Experiments on bulk alloys[18] show that the lro structure is not D1a, but the exact structure has not yet been identified. Thus, thin films and bulk alloys may behave differently, as has been shown in Au_3Mn.[19] In the present study the sro state was studied both in thin films and in foils made from bulk alloys. Since the important crystallographic features of the D1a structure have been described earlier, they need not be repeated here. Figures 8a and b show the [001] and [$\bar{1}$30] diffraction patterns respectively, obtained from a thin film of Au_3Cr, after aging for 67 hours at 270°C. The patterns consist of superlattice reflections due to the D1a structure (see Fig. 11), together with weak spots that are due to double diffraction. The spots marked 'T' in Fig. 8(b) are due to the fine {111} fcc twins that are invariably present in such epitaxially grown thin films. As the

ordered structure was heated in the microscope stage, the D1a spots suddenly became weak and the $\{1\frac{1}{2}0\}$ sro spots appeared around 330°C. This temperature is the same as that reported for T_c by Tanner et al.[5] for Au_3Cr. This critical temperature was a good check on the composition of the thin film. Figure 9(a) shows a [001] diffraction pattern obtained after holding for 30 minutes at 330°C ± 10°C. Diffuse peaks can be seen at $\{1\frac{1}{2}0\}$ spots and these are triangularly shaped with the edges extending towards neighboring D1a superlattice positions. In fact the area of the triangle covers almost the entire area outlined by the dotted lines in Fig. 1a. Figure 9b shows a $[\bar{1}30]$ pattern taken at 370°C. Similarly to the case of Ni_4Mo, here also the observed diffuse peaks (marked by arrows) are not entirely due to weak D1a spots but are elongated towards the projection of $\{1\frac{1}{2}0\}$ spots and have the shapes outlined by dotted lines in Fig. 1b. So here again the diffuse D1a peaks are not isolated from the diffuse $\{1\frac{1}{2}0\}$ maxima, but merge together with them. This gives rise to a tetrahedral distribution of the diffuse sro scattering centered about $\{1\frac{1}{2}0\}$, but enveloping D1a positions.

It has been reported[5] that the ordering reaction in bulk Au_3Cr is very sluggish and diffraction patterns do not show any evidence of lro even after annealing for 550 hours at 270°C. Thus, on fast quenching from above Tc it should be possible to retain the sro state without inducing any lro. In order to check this and also to compare the high temperature results described above on thin films with that of the bulk, samples of Au_3Cr were quenched from various temperatures above Tc. Figures 10a and b show [001] and $[\bar{1}30]$ diffraction patterns

respectively, obtained on specimens that were water quenched from 550°C. These patterns are very similar to the high temperature electron diffraction patterns shown in Fig. 9. The $\{1\frac{1}{2}0\}$ spots in the quenched samples (Fig. 10a) are sharper compared to those in diffraction patterns at T_c (Fig. 9a), but the shape remains more or less the same. The $[\bar{1}30]$ pattern (Fig. 10b) is also identical to the high temperature pattern shown in Fig. 9. Here again the diffuse peaks near D1a positions elongate towards the $\{1\frac{1}{2}0\}$ spots. In addition to the diffuse peaks there are extra spots due to relrods from the (111) and (200) reciprocal lattice points above and below this section.

In order to derive more conclusively the shape of the $\{1\frac{1}{2}0\}$ intensity distributions, some other reciprocal lattice sections were also examined. Figure 11(a) shows a [121] pattern that has been indexed in Fig. 11(b). The symbols used in indexing are the same as in Fig. 1. The D1a positions marked 3 and 4 in Fig. 11(b) are especially important in determining the shape of $\{1\frac{1}{2}0\}$ spots. Diffuse peaks can be observed near these and equivalent positions. They are elongated in the ⟨ 210 ⟩ directions shown by the full and dotted lines on the indexed pattern and are shifted in the direction of the arrows shown, which point towards the projection of the $\{1\frac{1}{2}0\}$ spots. The diffuse scattering near the D1a positions such as 1 and 2 are difficult to distinguish from the broad diffuse $\{1\frac{1}{2}0\}$ spot that lies very close to it. Based on the information gathered above, a three-dimensional reciprocal lattice model of the sro state was constructed and Fig. 12(a) shows the intensity distribution around each $\{1\frac{1}{2}0\}$ position. It can

be seen that each $\{1\frac{1}{2}0\}$ spot is stretched out into two triangular shaped sheets of intensity that are normal to each other. For comparison the three-dimensional reciprocal lattice of the fully ordered Dla structure is also shown in Fig. 12(b). It is clear that the shapes of the $\{1\frac{1}{2}0\}$ sro spots have resulted from interference due to weak scattering near the four Dla positions surrounding them.

The comparison of these results of quenched bulk samples with those obtained at T_c proves that no &ro has been induced in Au_3Cr during the quench. On this basis it is quite reasonable to assume that in the Ni-Mo alloys weak scattering is also present near Dla and Ni_2Mo superlattice positions in the sro state above Tc. The fast quenching may have slightly enhanced their intensities. High temperature electron diffraction patterns of thin films of Au_4Cr at 340°C ($T_c \sim 325$°C) were identical to those in Fig. 9 for Au_3Cr and showed diffuse scattering near Dla positions. Thus, Au_3Cr and Au_4Cr are similar to Ni_3Mo and Ni_4Mo in that they all have similar sro structures, although the &ro structure of Au_3Cr in thin films and bulk alloys may be different.

3.4. $\underline{Au_4V}$: The alloy Au_4V also possesses the Dla structure[20] in the &ro state and is disordered fcc above T_c (~565°C). So far there have been no reports of electron diffraction studies of order-disorder transformations in this system. Since this system is isostructural with Ni_4Mo and Au_4Cr it would be interesting to determine whether this alloy has a similar sro structure (diffuse $\{1\frac{1}{2}0\}$ reflections and weak superlattice reflections). Figure 13 shows a [001] electron diffraction

pattern of a bulk sample quenched in iced brine from 900°C. Weak peaks can be observed in this pattern at $\{1\frac{1}{2}0\}$ positions (marked by arrows). There is an enhanced scattering of each $\{1\frac{1}{2}0\}$ spot towards the neighboring Dla positions. As a matter of fact the diffuse intensity extends beyond the Dla position towards the fundamental fcc spots. Examination of other reciprocal lattice sections such as [121] and [$\bar{1}$30] confirms this observation. The reason for this is not quite clear at present, but in any case the important observation is that diffuse scattering is present near Dla positions. Although no diffraction patterns were examined at temperatures above T_c, comparison with the results on Au_3Cr suggests that quenching retains the sro state above T_c, fairly well in this alloy.

3.5. Au_3Mn: The bulk system Au_3Mn shows a DO_{22} structure [also described as a long period superlattice of the type $L1_2$ (M=1) i.e. an antiphase derivative of the Cu_3Au structure where an APB is introduced at every unit cell] with long period stacking modulations.[19] In thin films this alloy has a two-dimensional long period superstructure analyzed by Watanabe.[21] The alloy Au_4Mn forms the Dla structure both in thin films[22] and in bulk.[19,23] In the narrow composition range between 20 to 25 at.% Mn at least six different structures exist at various composition and temperature ranges. Consequently this alloy system is very interesting in order to see whether diffuse scattering above T_c shows any evidence for the presence of weak superlattice reflections corresponding to any of the complicated ordered structures observed below T_c.

Figure 14(a) shows a [001] diffraction pattern from an evaporated thin film of Au_3Mn showing only the Watanabe type two-dimensional long period superlattice and Fig. 14(b) shows a similar pattern but containing additional Dla spots, indicating a mixture of Au_4Mn and Watanabe type Au_3Mn, and that the films probably differ in composition. The [001] reciprocal lattice section corresponding to the Watanabe type structure is shown in Fig. 14(c), where the filled small circles are the superlattice spots corresponding to the two-dimensional long period superlattice with periodicities $m_1 = (\frac{a^*1}{M_1})$ and $m_2 = (\frac{a^*2}{M_2})$. Here a*1 and a*2 refer to the reciprocal lattice vectors and M_1 and M_2 correspond to the periodicities in real space in the a_1 and a_2 directions respectively. That is, in real space the periodic APB's occur at every M_1 and M_2 unit cells in the a_1 and a_2 directions respectively. The values of M_1 and M_2 determined from the diffraction patterns were found to be 1·2 and 2·3 respectively, which are close to those obtained by Watanabe.[21] In addition to the superlattice reflections there are weak satellites present (marked by small open circles) which are thought to arise from lattice modulations such as the variations in the lattice spacing or scattering factor and hence have the same periodicity as the APB's.[21]

The two different kinds of ordered states, one containing the two-dimensional long period superlattice [Fig. 14(a)] and the other a mixture of Dla and Watanabe type structure [Fig. 14(b)] were heated above T_c to examine if there are any differences in the diffuse scattering behavior. During heating, it was observed that the Dla spots

disappeared completely around 450°C and only the Watanabe type structure remained and Fig. 15(a) shows a diffraction pattern taken at 450°C. This pattern corresponds to the film that contained a mixture of Dla and Watanabe type structure in the ordered state before heating [Fig. 14(b)]. The streaks are still present at this temperature. On further heating to 475°C all the sharp superlattice reflections vanished and were replaced by diffuse scattering around $\{1\frac{1}{2}0\}$ positions and Fig. 15(b) shows the pattern taken at 500°C. The samples containing only the Watanabe type ordered structure, such as in Fig. 14(a), showed diffraction patterns above T_c that were identical to Fig. 15(b). Thus the sro state above T_c in these samples containing different initial ordered structures are identical. Although the actual composition of these films are unknown, the low T_c (475°C) suggests that the composition is closer to Au_4Mn than Au_3Mn. It can be seen from Fig. 15(b) that the diffuse intensity is not as concentrated around $\{1\frac{1}{2}0\}$ as was observed in Au-Cr and Ni-Mo alloys, but is fairly spread out in the ⟨100⟩ directions. Measurements show that the diffuse intensity extends from the superlattice position marked P [Fig. 14(c)] to that marked Q, which shows that there is diffuse scattering present near most of the superlattice reflections in Fig. 14(c), except those near A and C and their equivalent positions. If there is any scattering present near A and C it must be very weak. The shape of the diffuse scattering is quite different from that of Au_3Cr and shows no enhanced scattering towards the Dla positions. There is also no diffuse scattering observed near the satellite positions of Fig. 14(c).

Thus the diffuse scattering results above T_c in thin films of Au-Mn alloys of compositions between 20-25 at% Mn show the presence of weak scattering near most of the superlattice reflections of the Watanabe type two-dimensional long period superstructure.

4. DISCUSSION

The results of the sro alloys presented above show conclusively that in alloy systems that exhibit diffuse $\{1\frac{1}{2}0\}$ sro peaks, there is additional weak scattering present near the superlattice reflections, which are not isolated from the $\{1\frac{1}{2}0\}$ peaks but merge with them. In different systems the $\{1\frac{1}{2}0\}$ peak assumes different shapes, so as to give rise to scattering near these various superlattice positions. Now, first an attempt will be made to account for the various shapes of these diffuse $\{1\frac{1}{2}0\}$ spots by using the C-M model.[1] It will be seen that this model in its present form is unable to account for all the features of the observed diffuse scattering. Next it will be examined whether the structural interpretation of the sro state can explain the observed shapes or not.

4.1. Statistical Thermodynamic Model of SRO: In the high temperature approximation of the C-M model the diffuse intensity, $I(\bar{k})$ at any reciprocal lattice point, $\bar{k}$, can be written as

$$I(\bar{k}) = C\left[1 - \frac{T_c}{T} \cdot \frac{V(\bar{k})}{V(\bar{k}_m)}\right]^{-1} \qquad (1)$$

where C is a normalization constant, T_c is the critical temperature for order-disorder transitions T is any temperature above T_c where the diffuse scattering is measured, and $V(\bar{k})$ is the Fourier transform of the pairwise interaction potential. For a fcc crystal, considering the interaction potentials Vi's only up to third nearest neighbors $V(\bar{k})$ can be written as,

$$\begin{aligned} V(k) = {} & 4V_1 [\cos \pi h_1 \cos \pi h_2 + \cos \pi h_2 \cos \pi h_3 + \cos \pi h_3 \cos \pi h_1] \\ & + 2V_2 [\cos 2\pi h_1 + \cos 2\pi h_2 + \cos 2\pi h_3] \\ & + 8V_3 [\cos 2\pi h_1 \cos \pi h_2 \cos \pi h_3 + \cos \pi h_1 \cos 2\pi h_2 \cos \pi h_3 \\ & + \cos \pi h_1 \cos \pi h_2 \cos 2\pi h_3] \end{aligned}$$

where $\{h_1, h_2, h_3\}$ are continuous variables in reciprocal space. $V(\bar{k}_m)$ corresponds to the value of $V(\bar{k})$ at that position in reciprocal lattice, $\bar{k}_m$, where it takes an absolute minimum value. The intensity $I(\bar{k})$ has a peak where $V(\bar{k})$ goes to a minimum and in the present case, since we are concerned with the diffuse peaks at $\{1\frac{1}{2}0\}$ positions, the value of $V(k_m)$ is the value at $h_1 = 1$, $h_2 = \frac{1}{2}$, $h_3 = 0$. Using Eq. (1) iso-intensity contours were plotted for all possible values of the ratios $\frac{V_2}{V_1}$ and $\frac{V_3}{V_1}$ keeping a constant $\frac{T_c}{T} = 0.95$ close to the experimental value. No matter what values of the ratios of the interaction parameters were chosen, it was not possible to match the computed shape with the tetrahedral shape of $\{1\frac{1}{2}0\}$ sro spots in Au-Cr alloys [Fig. 12(a)] and also in Au_4V. In the case of Ni_4Mo, Clapp and Moss tried to match the computed curves with the X-ray results of Spruiell and Stansbury and obtained good agreement. But as pointed out earlier, the X-ray

results failed to detect any scattering near D1a positions and so also did the computations. Similar attempts were made to obtain a match for Ni_3Mo and Fig. 16 shows the best possible match with that of Fig. 6(a), by using $\frac{T_c}{T} = 0.95$, $\frac{V_2}{V_1} = 0.4$ and $\frac{V_3}{V_1} = 0.00$. The intensities are in relative units. Here, although the diffuse scattering near Ni_2Mo positions is reproduced well in the computed curve, it is still not possible to obtain any scattering near D1a positions.

The shapes of the $\{1\frac{1}{2}0\}$ spots in Au_3Mn [Fig. 15(b)] are quite different from other systems as they are in the form of a cigar elongated along ⟨100⟩. The theoretical diffuse scattering map obtained by Moss and Clapp[2] for Au_3Mn using $\frac{V_2}{V_1} = +0.08$ does not match very well with our experimental result. A better match was obtained by using a large negative $\frac{V_2}{V_1} = -0.7$ and $\frac{V_3}{V_1} = -0.2$ as shown in Fig. 17.

These results show that the statistical model, can explain the diffuse scattering results very well for Au_3Mn, partially for Ni-Mo alloys, but not for Au_3Cr, Au_4Cr and Au_4V. Clapp[24] has suggested that this failure may be due to the fact that equation (1) is only a high temperature approximation and in the region near T_c the linear approximation is poor. The other possibility is that one may need to incorporate higher order interaction parameters (V_{ij} beyond V_3) in order to fully account for the shapes of $\{1\frac{1}{2}0\}$ diffuse spots. In the following section it will be shown that the structural model can qualitatively account for the observed results and at the same time gives a better physical description of the sro state than the statistical theory.

4.2. Structural Interpretation of the SRO State: Any structural model for the sro state in the systems investigated has to account for the presence of all the weak superlattice reflections observed, and the $\{1\frac{1}{2}0\}$ spots. There are two structures, namely the DO_{22} and $L1_0$ (M = 1) that give rise to superlattice reflections at $\{1\frac{1}{2}0\}$ positions in the fcc reciprocal lattice. A perfectly ordered DO_{22} structure exhibits superlattice peaks at $\{1\frac{1}{2}0\}$ and also at {100} positions but the experimental results do not show any diffuse peaks at {100} positions. It has been shown[8] that if there exists a sinusoidal composition fluctuation within the DO_{22} structure the {100} reflections are extinct and thus the diffuse sro peaks at $\{1\frac{1}{2}0\}$ positions have been interpreted in terms of imperfectly ordered microdomains.

It may seem equally likely that the sro state may have microdomains with $L1_0$(M = 1) structure, which also give rise to peaks at $\{1\frac{1}{2}0\}$ positions, Although this structure is rarely observed in ordered alloys, recently Lin et al.[25] have indicated that this structure might exist in Au-40 at% Pd alloy. In the composition range (20-25 at% solute) investigated the probability of occurrence of the $L1_0$(M = 1) structure, which corresponds to 50 at% solute will be less than that for the DO_{22} structure containing 25 at% solute, because the presence of $L1_0$(M = 1) type microdomains in a sample with 20-25 at% solute will also necessarily mean the existence of very large composition fluctuations. Thus, it is more likely that the imperfectly ordered microdomains with DO_{22} structure are responsible for the diffuse $\{1\frac{1}{2}0\}$ spots, and this choice

will be further justified later.

The presence of weak scattering near Dla positions in Au_3Cr, Au_4Cr, Au_4V, Ni_4Mo and Ni_3Mo in the sro state can be due to the presence of microdomains with Dla structure. In the Ni_4Mo and Ni_3Mo alloys there is additional diffuse scattering present near Ni_2Mo positions which implies that there are microdomains with Ni_2Mo type superstructure. Since no superlattice reflections were detected at Ni_3Mo positions, there may not be any microdomains present with the Ni_3Mo structure, although this is the equilibrium lro structure of stoichiometric Ni_3Mo. Thus, it appears that in the sro state, Au_3Cr, Au_4Cr and Au_4V alloys contain predominantly microdomains of imperfectly ordered DO_{22} and Dla structures, whereas in Ni_4Mo and Ni_3Mo additional microdomains of Ni_2Mo type structure will exist. The reason Ni_2Mo type microdomains do not exist in Au-Cr and Au-V alloys is probably because there is no ordered phase in these systems with Ni_2Mo type structure. The atomic size effects may also be very important in deciding what structures will exist in the sro state. The three structures DO_{22}, Dla and Ni_2Mo are very closely related to each other and, starting with any one of these, the two others can be derived by simply introducing a periodic distribution of $\{420\}\frac{1}{2}\langle\bar{1}10\rangle$ type APB's.[8,15] In the sro state above T_c if diffusion is fast enough, tiny regions with these various types of closely related ordered structures may be continuously forming and disappearing in order to establish an equilibrium distribution. Statistically, there exists a finite probability for some other closely related structures to exist

other than the above three, but their volume fraction may be very small to give rise to any appreciable diffraction effect. At a particular stoichiometry the entire sample may consist of such imperfectly ordered microdomains with various volume fractions in order to balance the composition. The degree of order within these various types of microdomains must be very low as it was impossible to obtain contrast in dark field images of these diffuse spots. On quenching fast enough from above T_c, the high temperature distribution of various types of microdomains is essentially retained. However, depending on the quenching rate, the degree of order within these microdomains may be slightly enhanced as is indicated by the intensities of Dla spots in diffraction patterns of quenched Au_3Cr compared to those taken above T_c. The evidence for the presence of various types of microdomains is primarily based on their diffraction effects. Although the dark field micrographs do not reveal directly the microdomains when the spots are very diffuse, they do reverse contrast for respective microdomains after short time aging when the degree of order has increased slightly. For example the microdomains observed in Fig. 7(a) in the dark field of the $\{1\frac{1}{2}0\}$ spot may consist of predominantly imperfectly ordered DO_{22} regions. Recently Penisson et al.[26] have obtained evidence for microdomains in dark field images of the diffuse {100} spots in Pt-Co alloy quenched from above T_c.

The above discussion leads us to propose a structural model of the sro state that is different from the classical microdomain concept where the structure of microdomains was simply assumed to correspond to the equilibrium lro structure. In this modified microdomain concept the sro state consists of not one but several types of microdomains

whose structures do not necessarily correspond to the equilibrium ℓ_{ro} structure. In some cases, as in Ni_3Mo, the equilibrium ℓ_{ro} structure may not exist at all in the sro state. This is very similar to Clapp's PVM calculation results,[9] mentioned earlier, where for the sro state in Au_3Cu he found the most enhanced cluster type to be CuAu, and not Au_3Cu. Also the above description of the sro state supports Clapp's calculations that clusters may be present corresponding to different superstructures. Unfortunately, for the systems investigated in this work there are no three-dimensional sro parameters available, and so such PVM calculations cannot be performed. However, there are some three-dimensional sro parameters available[27] for Ni-10 at% W, an alloy which is quite similar to Ni-Mo. Clapp's calculations[24] using the sro parameters of Ni-10 at% W show the most enhanced cluster to be the DO_{22} type. The next most enhanced cluster is the D1a with one mistake. It is not unreasonable to expect a similar distribution in Ni-Mo alloys and so the previous choice for the DO_{22} type microdomains to be present in the sro state of Au-Cr, Au-V, and Ni-Mo alloys instead of $L1_0$ (M = 1) type seems to be well justified.

The results of diffuse scattering in Au_3Mn can also be explained qualitatively by structural models. The cigar shaped $\{1\frac{1}{2}0\}$ spots give rise to diffuse scattering at the superlattice reflections P, Q, R, S and their equivalent spots [Fig. 14(c)]. The superlattice reflections in Fig. 14(c) can be thought of as formed by the splitting of the reciprocal lattice points with mixed integers h_1, h_2, 0, the splitting distance being $\pm \frac{m_1}{2}$ along $[h_1 00]$ and $\pm \frac{m_2}{2}$ along $[0h_2 0]$,

which arise from the presence of periodic APB's at every M_1 ($= \frac{a_1^*}{m_1}$) and M_2 ($\frac{a_2^*}{m_2}$) cells along the respective directions, as described earlier in sec. 3.5. At temperatures above T_c, if there exist microdomains with the Watanabe type structure, but without any fixed periodicities M_1 and M_2, then there will be no strong superlattice reflections, but a broad diffuse scattering near positions corresponding to all possible periodicities that are present as observed in Fig. 15(b). Since the origin of the satellites in Fig. 14(c) is most likely to be due to periodic lattice modulations or composition modulations in the lro state, these will be completely washed out in the sro state because there will be hardly any such periodic modulation present. This explains the absence of any scattering near satellite positions above T_c. Thus the diffuse scattering in Au_3Mn can also be accounted for by the presence of microdomains with Watanabe type structure. The presence of the microdomains of such long period Watanabe type structure in the sro state would necessarily imply that long range interatomic interactions are present. The justification for long range interactions being present in the sro state has been given by Cowley[28] in terms of flat regions being present on the Fermi surface.

5. CONCLUSIONS

1. The high temperature electron diffraction patterns of Au_3Cr and Au_4Cr above T_c show a tetrahedral intensity distribution around the $\{1\frac{1}{2}0\}$ positions which gives rise to diffuse scattering at Dla positions. The comparison of the as quenched state with diffraction patterns taken

above T_c show that the sro state is essentially retained on quenching in this alloy.

2. The diffraction patterns of Au_4V in the sro state also exhibit diffuse scattering at $\{1\frac{1}{2}0\}$ and Dla positions.

3. The diffuse scattering in Au_3Mn above T_c gives rise to an intensity distribution centered around $\{1\frac{1}{2}0\}$ in such a way that weak scattering is present near most of the superlattice reflections corresponding to Watanabe type two dimensional long period superstructure.

4. The sro states of Ni_4Mo and Ni_3Mo show diffuse scattering near Dla and Ni_2Mo superlattice positions in addition to those at $\{1\frac{1}{2}0\}$ positions.

5. The presence of weak scattering near various superlattice positions suggests that in the sro state, Au-Cr and Au-V alloys contain predominantly imperfectly ordered DO_{22} and Dla type microdomains. The Ni-Mo alloys contain imperfectly ordered DO_{22}, Dla and Ni_2Mo type microdomains whereas Au-Mn alloys may contain microdomains with a structure close to that of the Watanabe type long period superstructure.

6. The existing statistical thermodynamic model of Clapp and Moss is unable to explain the shape of $\{1\frac{1}{2}0\}$ spots in Au-Cr and Au-V alloys but can explain most features of diffuse scattering in Au-Mn and Ni-Mo alloys.

7. The classical microdomain concept is not always valid and the sro state may contain more than one type of microdomain. A modified microdomain model is proposed in which the sro state is best described as a mixture of imperfectly ordered microdomains with various types of superstructures in different proportions. This description of sro state is very similar to Clapp's description in terms of clusters.

ACKNOWLEDGEMENTS

This work was supported by the U. S. Atomic Energy Commission through the Inorganic Materials Research Division, Lawrence Berkeley Laboratory, University of California, Berkeley, California. The authors are grateful to Dr. L. E. Tanner for supplying the Au-Mn samples and for helpful discussions and to Dr. P. C. Clapp for his valuable comments.

REFERENCES

1. P. C. Clapp and S. C. Moss, Phys. Rev., 171, 754 (1968).
2. S. C. Moss and P. C. Clapp, Phys. Rev., 171, 764 (1968).
3. J. E. Spruiell and E. E. Stansbury, J. Phys. Chem. Solids 26, 811 (1965).
4. H. G. Baer, Z. Metallkde, 57, 318 (1966).
5. L. E. Tanner, P. C. Clapp and R. S. Toth, Mat. Res. Bull., 3, 855 (1968).
6. J. R. Castles, J. M. Cowley and A. E. C. Spargo, Acta Cryst. A27, 376 (1971).
7. P. R. Okamoto, Ph.D. Thesis, University of California, Berkeley UCRL-19175 (1969).
8. P. R. Okamoto and G. Thomas, Acta Met., 19, 825 (1971).
9. P. C. Clapp, Tech. Rep. No. 249, Ledgemont Laboratory, Kennecott Copper Corporation (1970).
10. P. C. Clapp, J. Phys. Chem. Solids, 30, 2589 (1969).
11. G. Thomas in High Temperature, High Resolution Metallography, Gordon and Breach Science Publishers, N.Y., 217 (1967).
12. D. Harker, J. Chem. Phys., 12, 317 (1944).
13. E. Ruedl, P. Delavignette and S. Amelinckx, Phys. Status Solidi 28, 305 (1968).
14. M. Yamamoto, S. Nenno, T. Saburi and Y. Mizutani, Trans. J.I.M., 11, 120 (1970).
15. S. K. Das and G. Thomas (submitted to Phys. Stat. Solidi).
16. S. Saito and P. A. Beck, Trans. AIME, 215, 938 (1959).

17. E. Ruedl and S. Amelinckx, Mat. Res. Bull., 4, 361 (1969).

18. S. K. Das, Ph.D. thesis, U. C. Berkeley, LBL-176 (1971).

19. H. Sato, R. S. Toth, and G. Honjo, J. Phys. Chem. Solids, 28, 137 (1967).

20. E. Stolz and K. Schubert, Z. Metallkde, 53, 433 (1962).

21. D. Watanabe, J. Phys. Soc. Japan, 15, 1030 (1960).

22. D. Watanabe, J. Phys. Soc. Japan, 15, 1251 (1960).

23. D. P. Morris and J. L. Hughes, Acta Cryst., 15, 1062 (1962).

24. P. C. Clapp (private communication).

25. W. Lin, J. E. Spruiell and R. O. Williams, J. Appl. Cryst. 3, 297 (1970).

26. J. M. Penisson, A. Bourret and Ph. Eurin, Acta Met., 19, 1195 (1971).

27. A. M. Ammons and J. E. Spruiell, J. Appl. Phys. 39, 3682 (1968).

28. J. M. Cowley in The Chemistry of Extended Defects in Non-metallic Solids, Eds. L. Eyring and M. Okeeffe, North Holland, London 259 (1970).

FIGURE CAPTIONS

Fig. 1. (a) [001] reciprocal lattice section containing Dla, Ni_2Mo, $\{1\frac{1}{2}0\}$ sro spots, (b) $[\bar{1}30]$ reciprocal lattice section.

Fig. 2. [001] diffraction pattern of Ni_4Mo quenched in iced brine from 1100°C.

Fig. 3. Iso-intensity contour map of the [001] electron diffraction pattern of quenched Ni_4Mo. The dotted line outlines the portion traced, and the notations for Ni_2Mo and Ni_4Mo positions are the same as in Fig. 1.

Fig. 4. $[\bar{1}30]$ electron diffraction pattern of quenched Ni_4Mo.

Fig. 5. (a) [110] diffraction pattern of Ni_4Mo. (b) the indexed pattern.

Fig. 6. Diffraction patterns of Ni_3Mo after quenching in iced brine from 1270°C (a) [001] pattern (b) [110] pattern.

Fig. 7. Ni_3Mo samples after aging for 1 hour at 650°C (a) Dark field micrograph of $\{1\frac{1}{2}0\}$ spot encircled in the diffraction pattern; (b) the $[1\bar{2}0]$ diffraction pattern corresponding to (a).

Fig. 8. Evaporated thin film of Au_3Cr after aging for 67 hrs at 270°C (a) [001] orientation, (b) $[\bar{1}30]$ orientation.

Fig. 9. (a) [001] diffraction pattern of Au_3Cr film taken at 330° ± 10°C; (b) $[\bar{1}30]$ pattern of same Au_3Cr film taken at 370°C.

Fig. 10. Electron diffraction patterns of bulk Au_3Cr after quenching in water from 550°C. (a) [001] pattern, (b) $[\bar{1}30]$ pattern.

Fig. 11. (a) [121] diffraction pattern of bulk Au_3Cr, quenched into water (b) the indexed pattern.

Fig. 12. Three-dimensional reciprocal lattice models of Au_3Cr showing (a) the distribution of diffuse scattering in the sro state, (b) the six variants of Dla in the &ro state.

Fig. 13. [001] diffraction pattern of bulk Au_4V quenched in iced brine from 900°C.

Fig. 14. (a) [001] diffraction pattern of evaporated thin film of Au_3Mn showing two-dimensional long period superstructure (Watanabe type), (b) another [001] pattern showing additional Dla superlattice spots, (c) sketch of [001] pattern corresponding to Watanabe type structure.

Fig. 15. (a) [001] diffraction pattern of ordered thin film of Au_3Mn taken at 450°C, (b) the same pattern as (a) but taken at 500°C.

Fig. 16. Theoretical diffuse scattering map for Ni_3Mo.

Fig. 17. Theoretical diffuse scattering map for Au_3Mn.

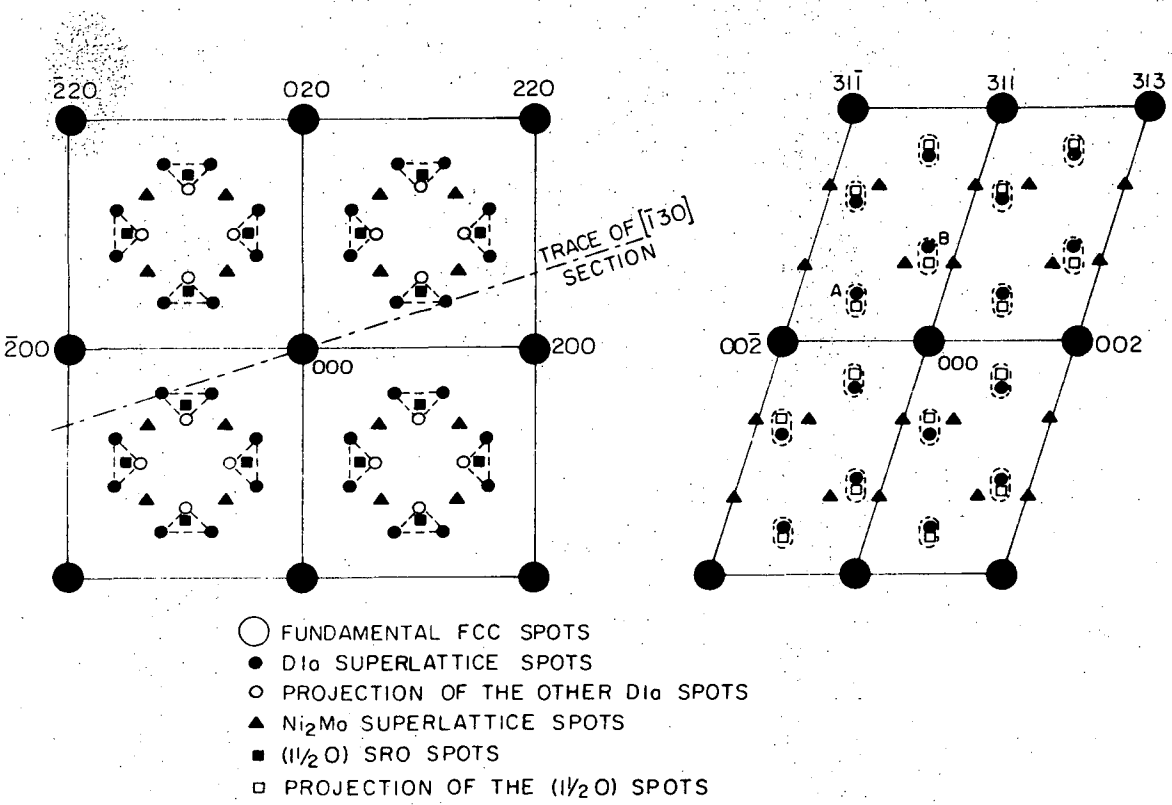
$\bar{2}20$
020
220
$\bar{2}00$
000
200
TRACE OF [$\bar{1}$30] SECTION
$31\bar{1}$
311
313
A
B
$00\bar{2}$
000
002
FUNDAMENTAL FCC SPOTS
D1a SUPERLATTICE SPOTS
PROJECTION OF THE OTHER D1a SPOTS
Ni_2Mo SUPERLATTICE SPOTS
(1½ 0) SRO SPOTS
PROJECTION OF THE (1½ 0) SPOTS
XBL717-7009

Fig. 1

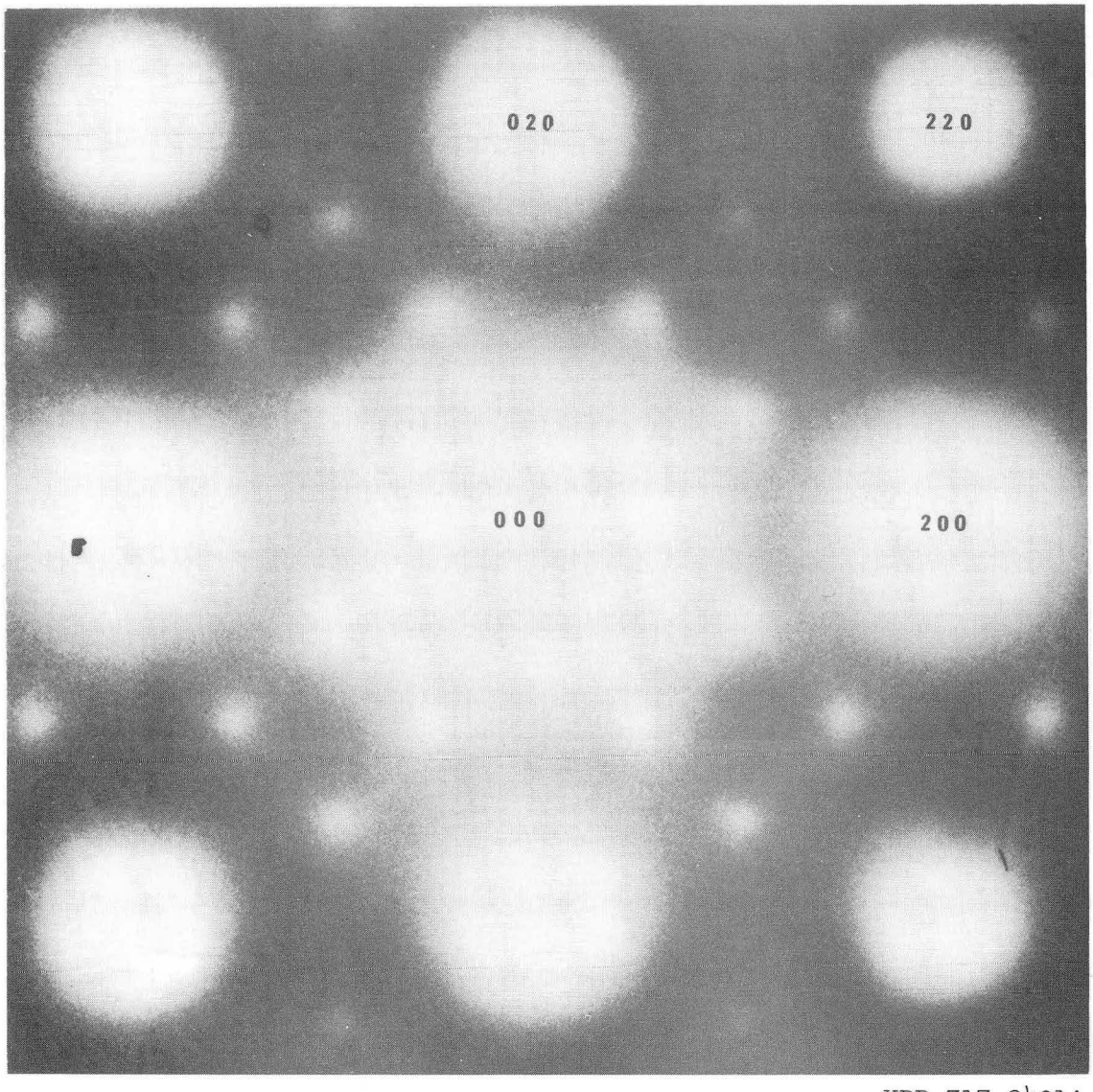

XBB 717-3401A

Fig. 2

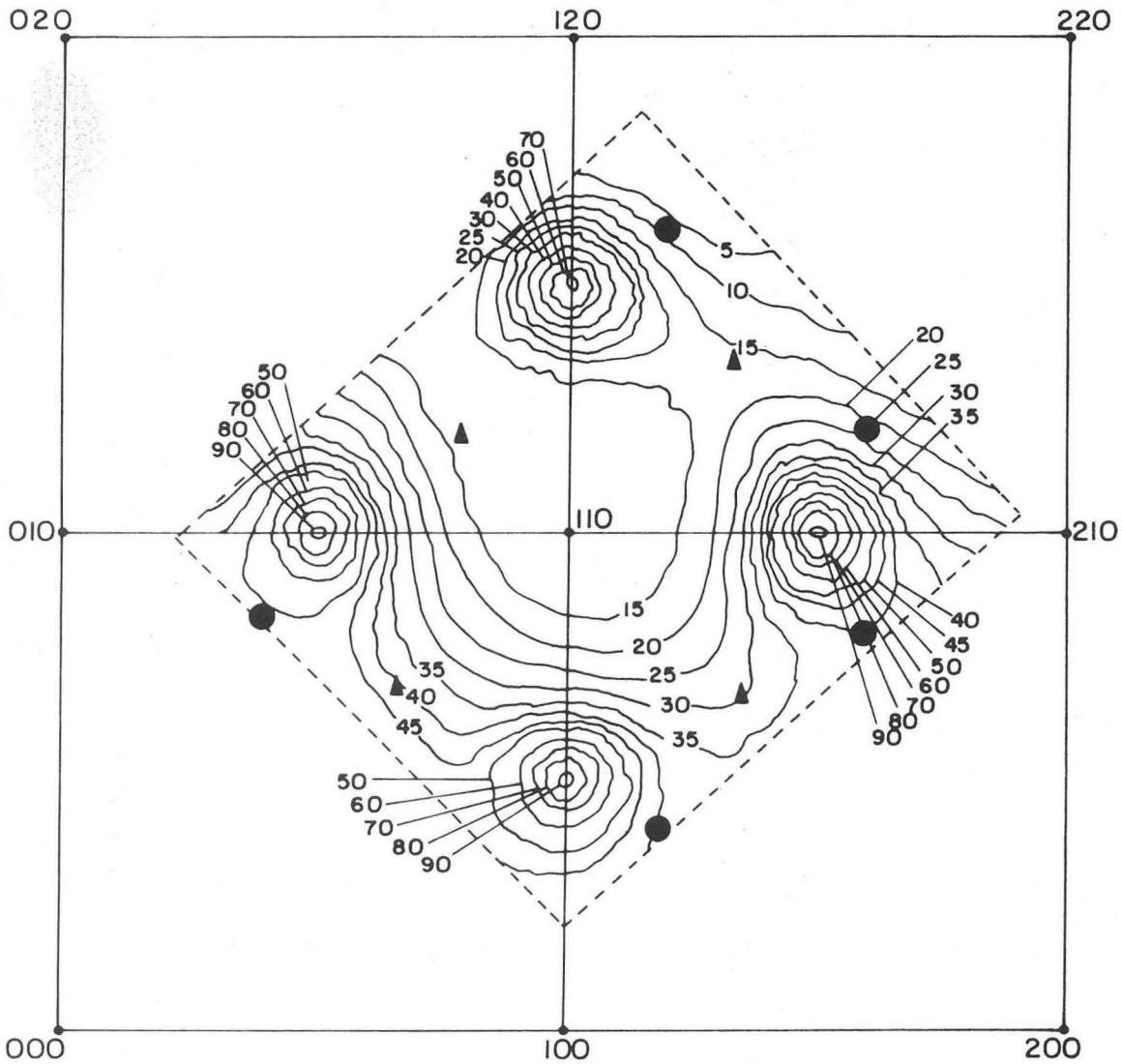

XBL7110-7338

Fig. 3

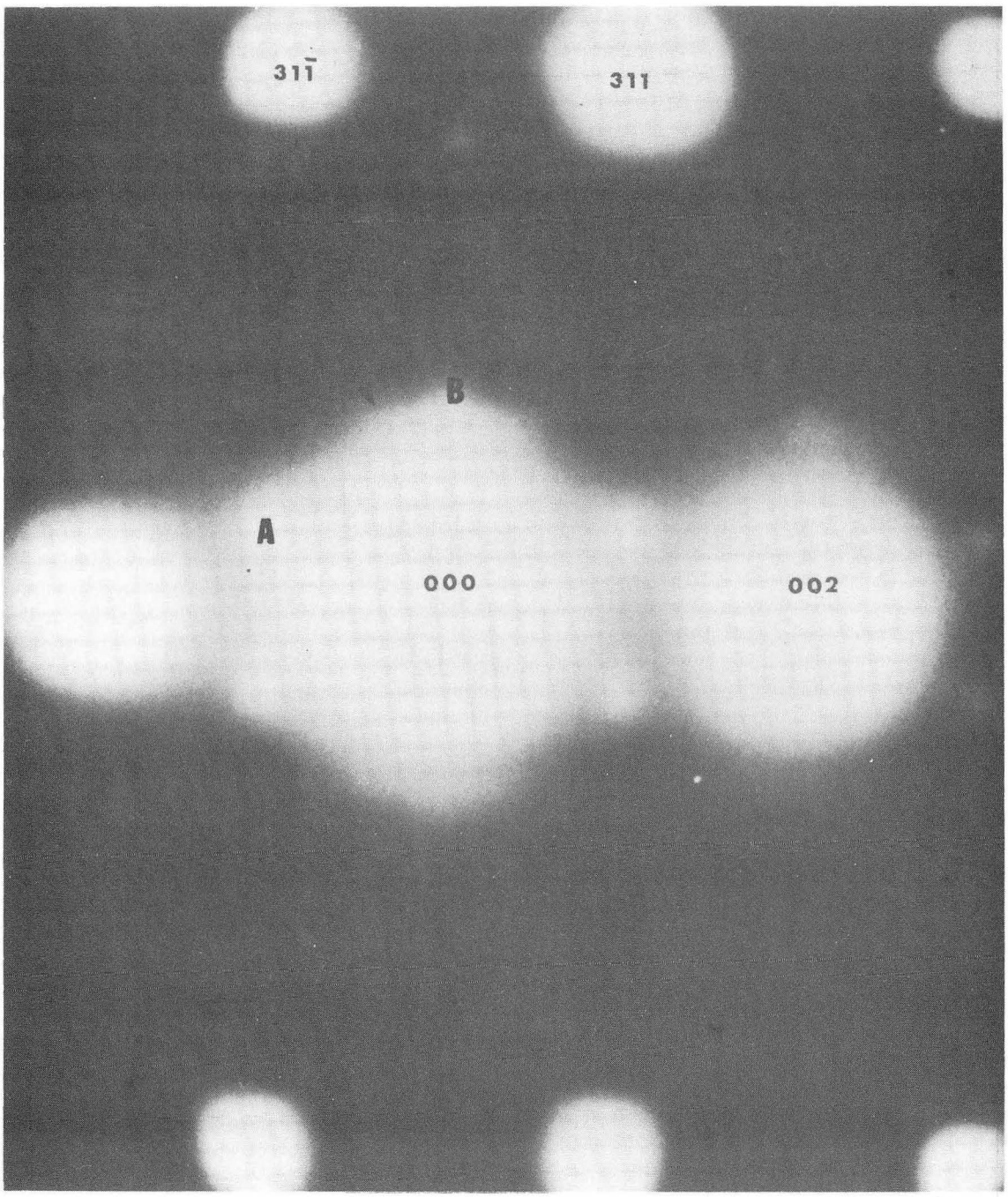

XBB 717-3407A

Fig. 4

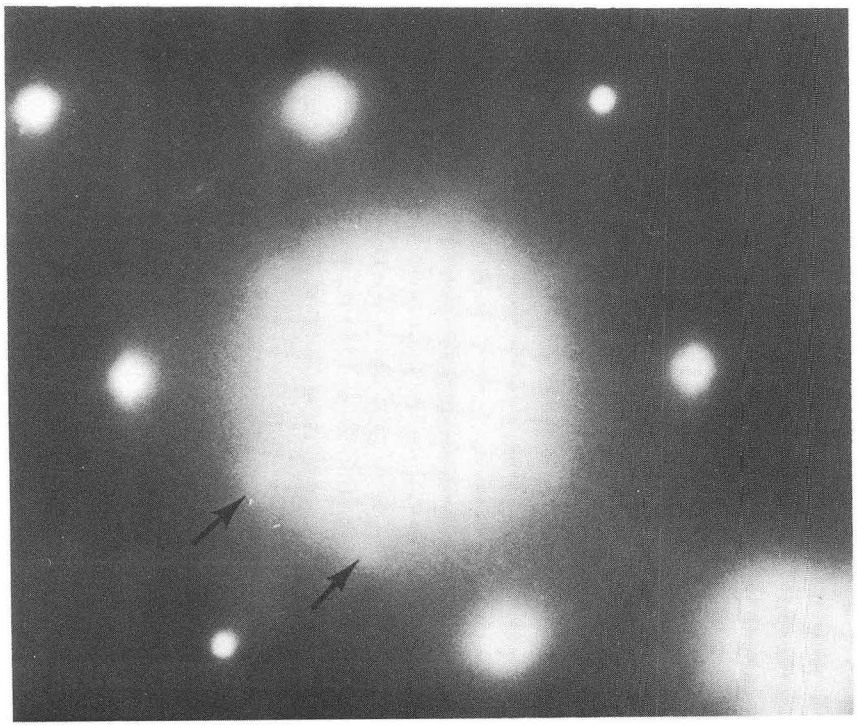

A

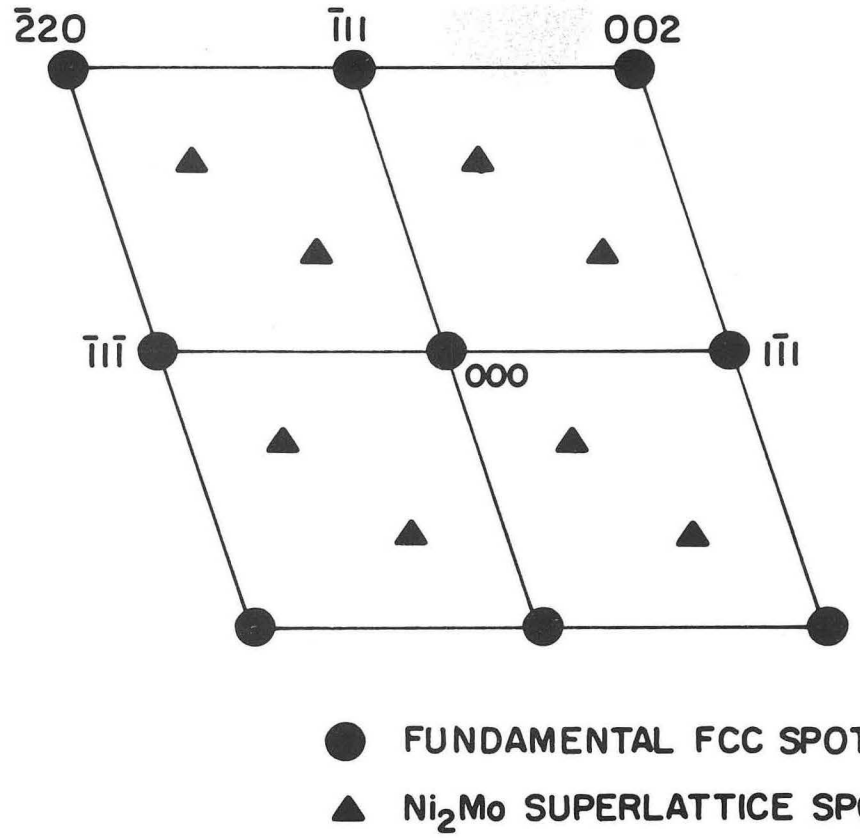

B

XBB 717-3397

Fig. 5

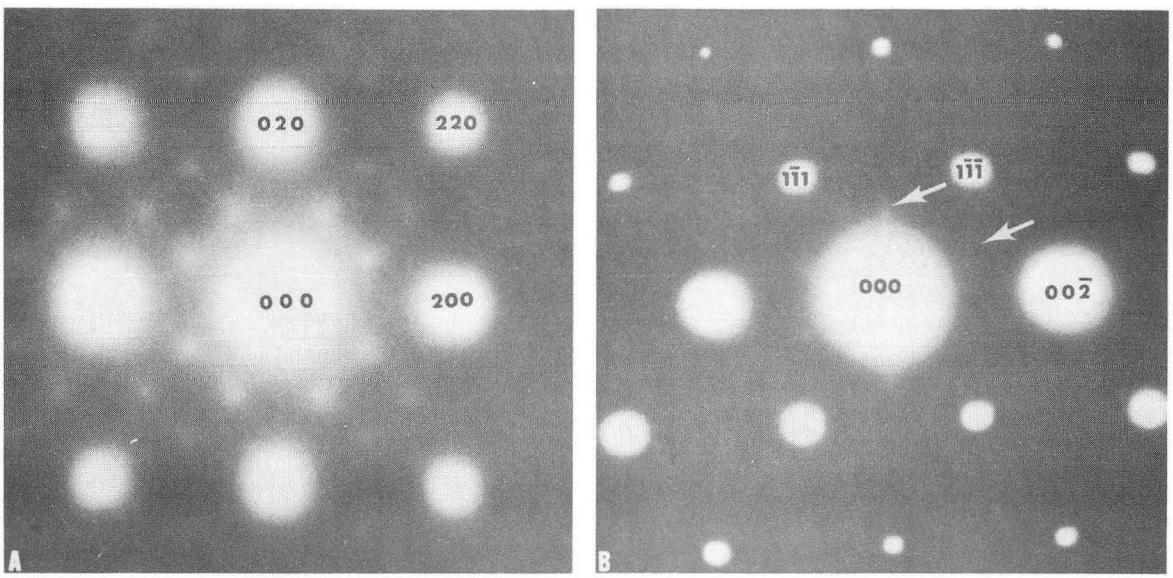

XBB 717-3406A

Fig. 6

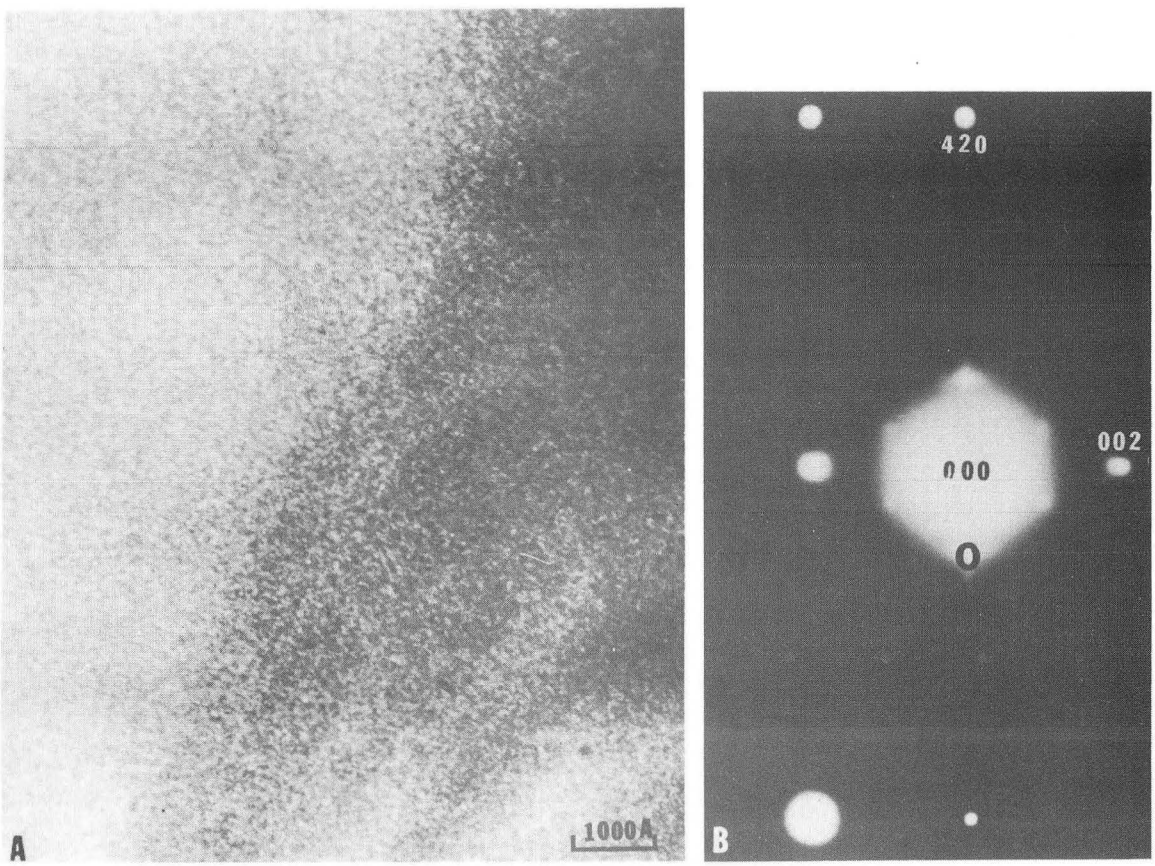

XBB 7110-4766A

Fig. 7

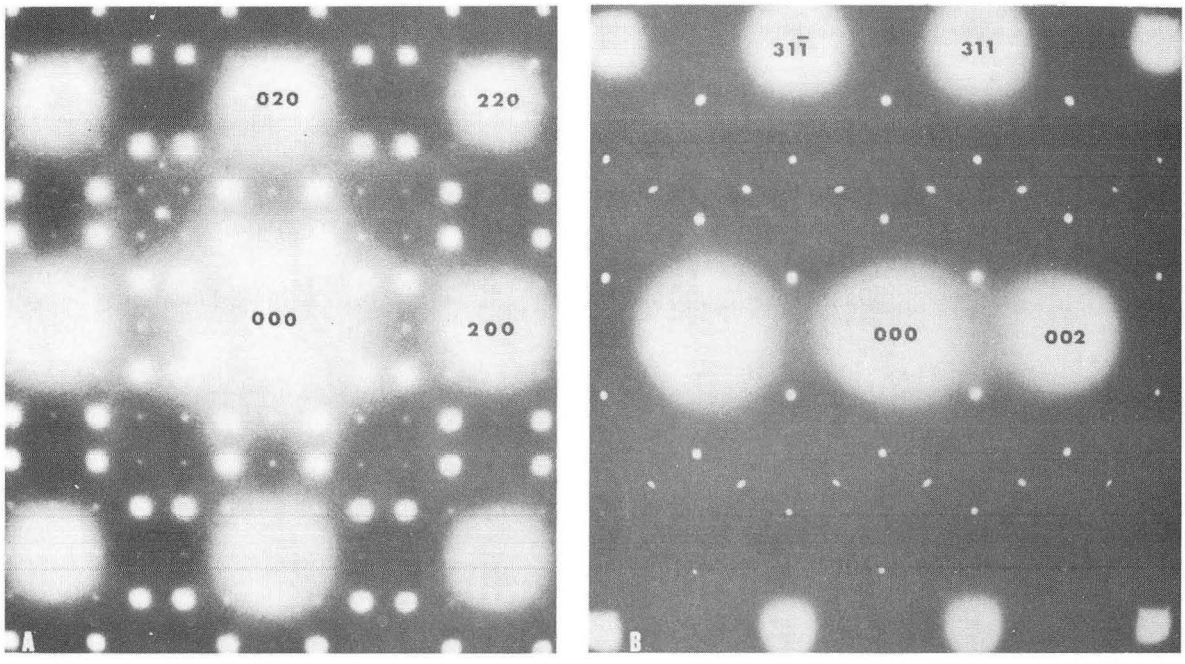

XBB 717-3405A

Fig. 8

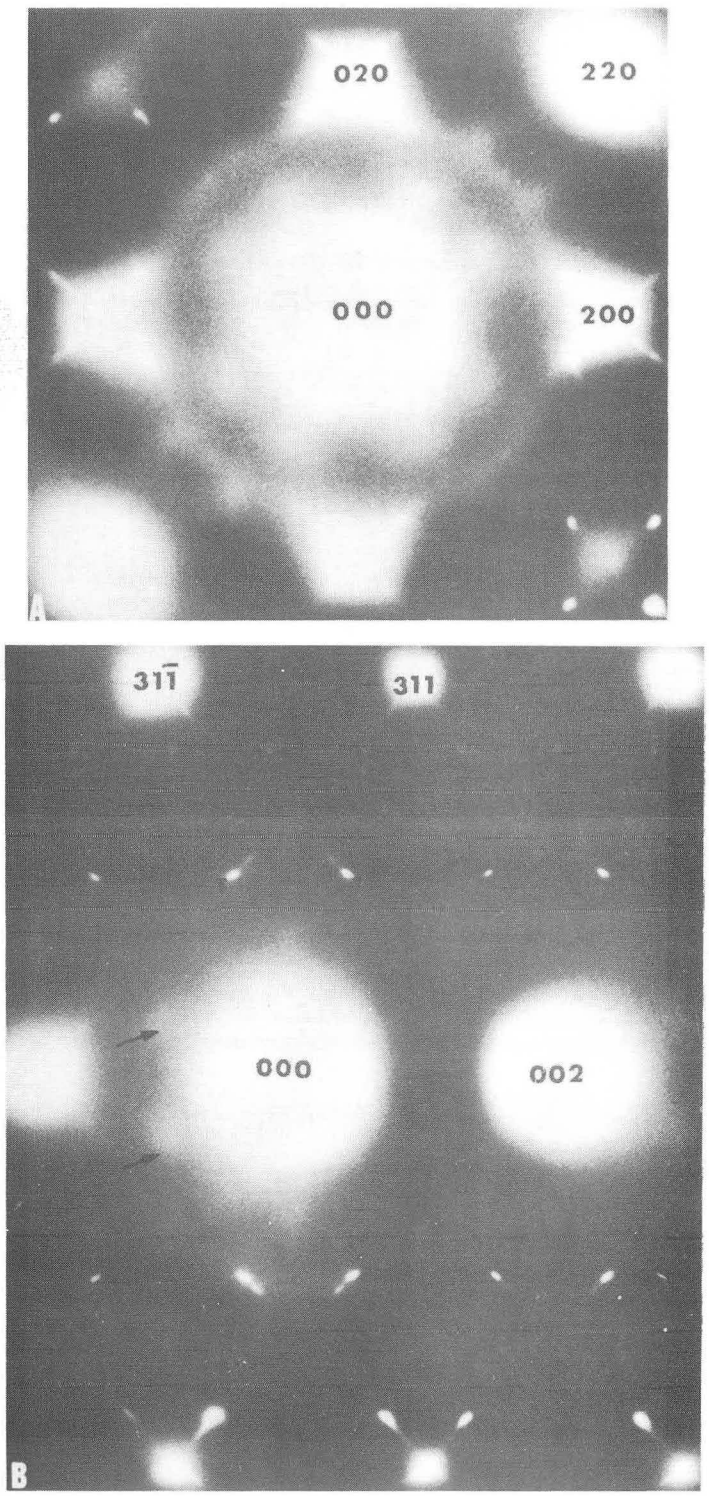

XBB 717-3401A

Fig. 9

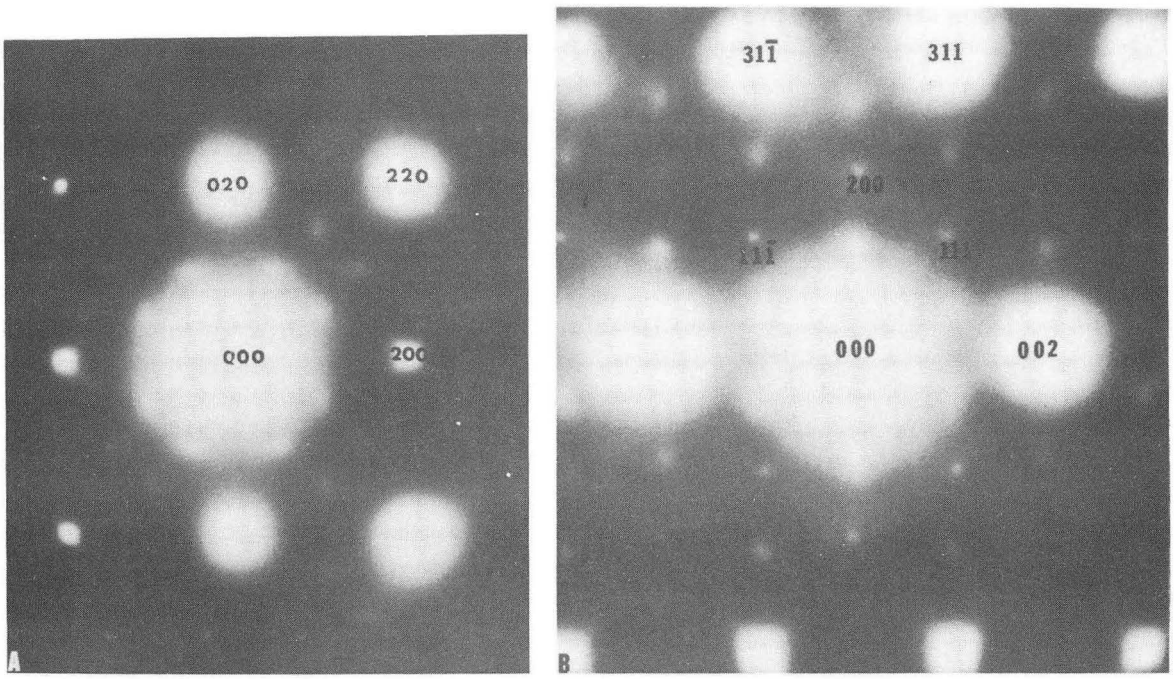

XBB 717-3404A

Fig. 10

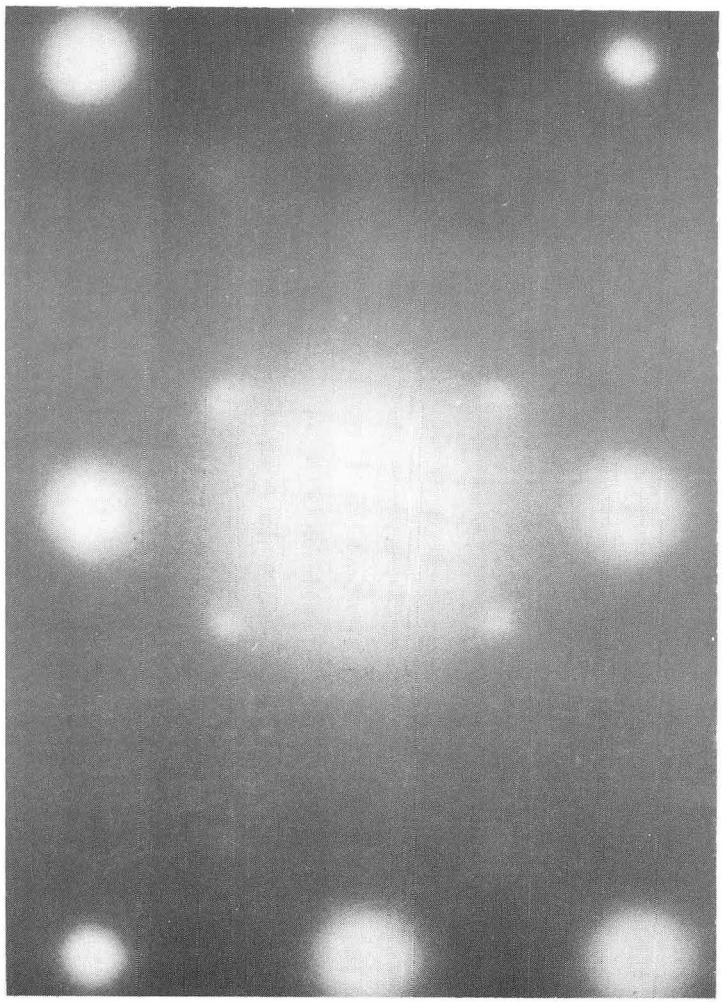

A

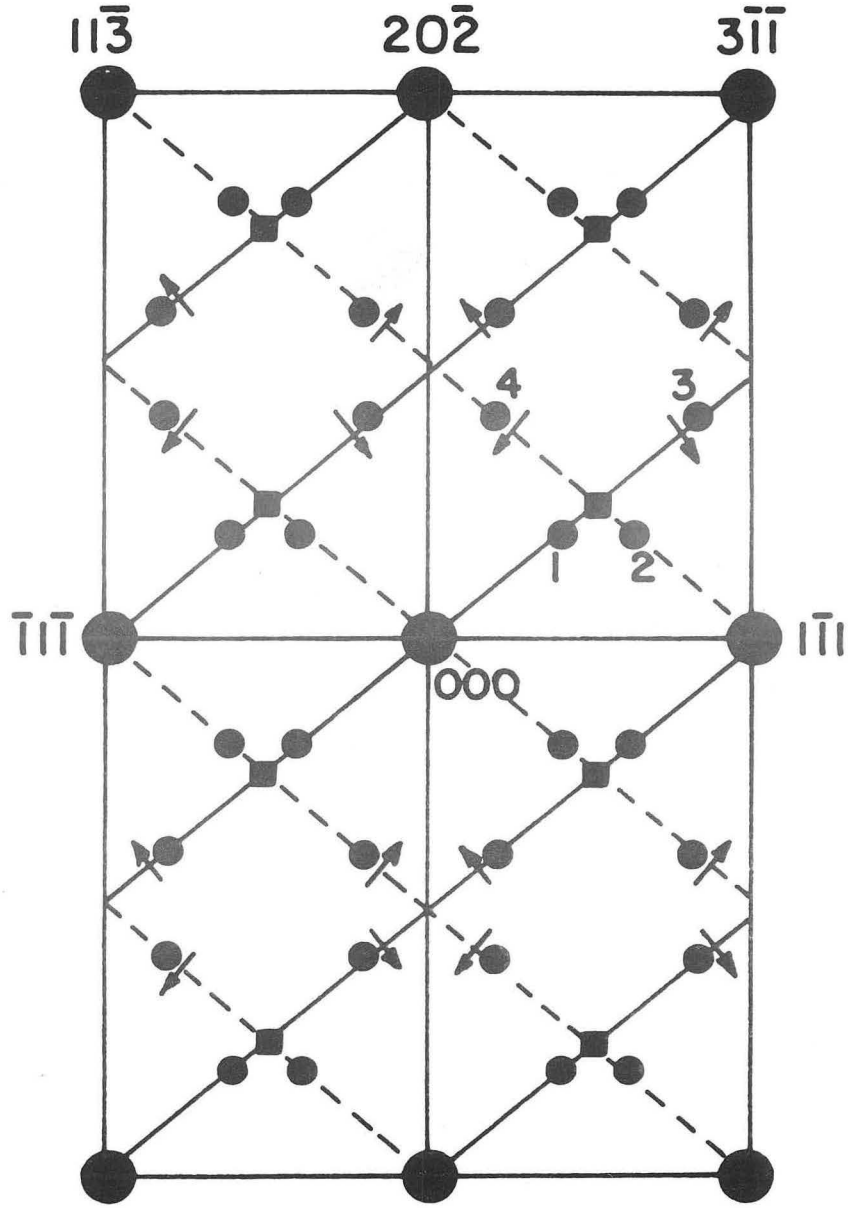

B

XBB 717-3396

Fig. 11

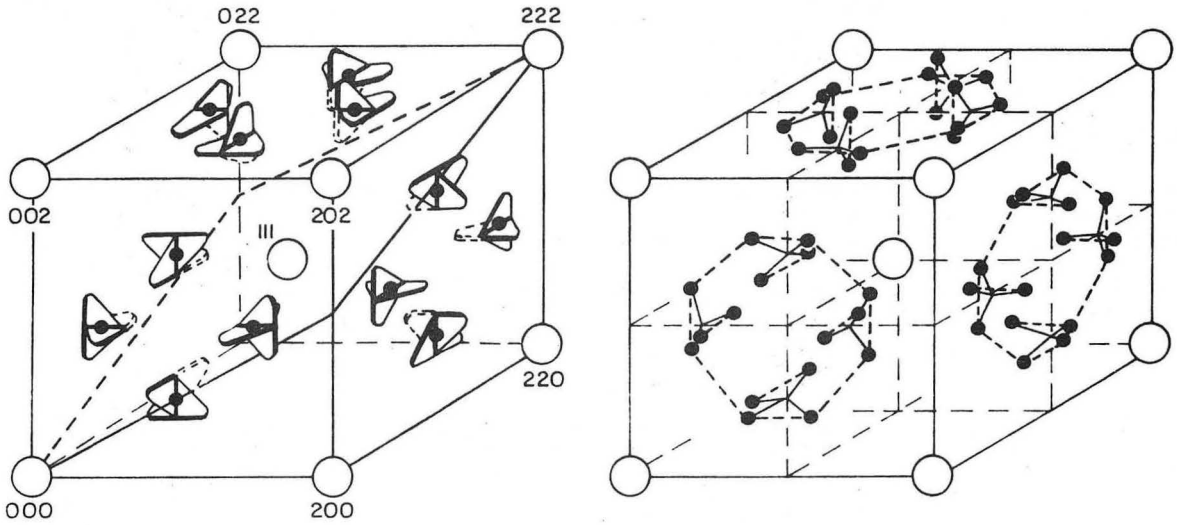

Disordered state

LRO state: 6 variants of D1a

Reciprocal lattices of Au_3Cr

XBL713-6626

Fig. 12

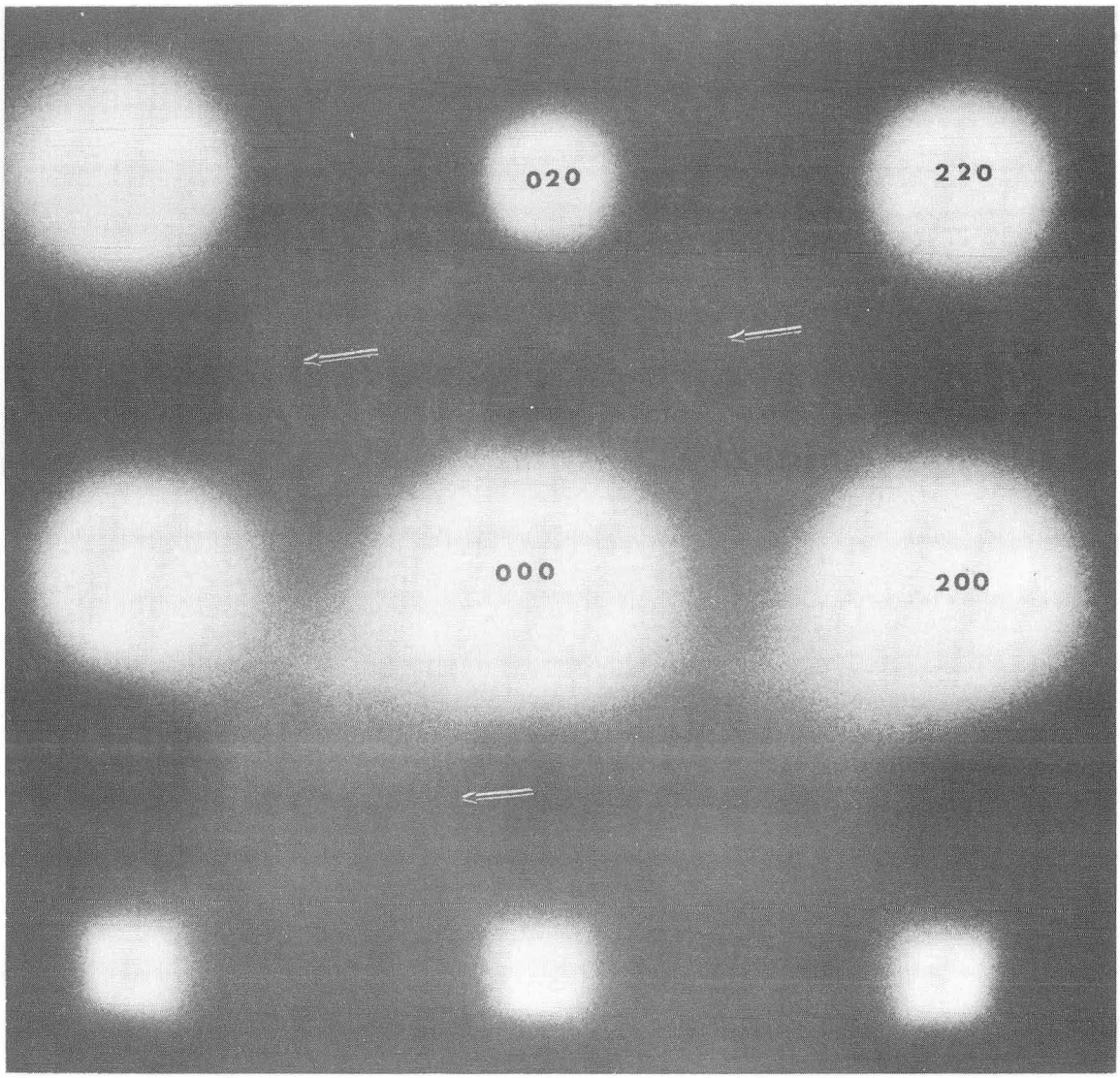

XBB 717-3399A

Fig. 13

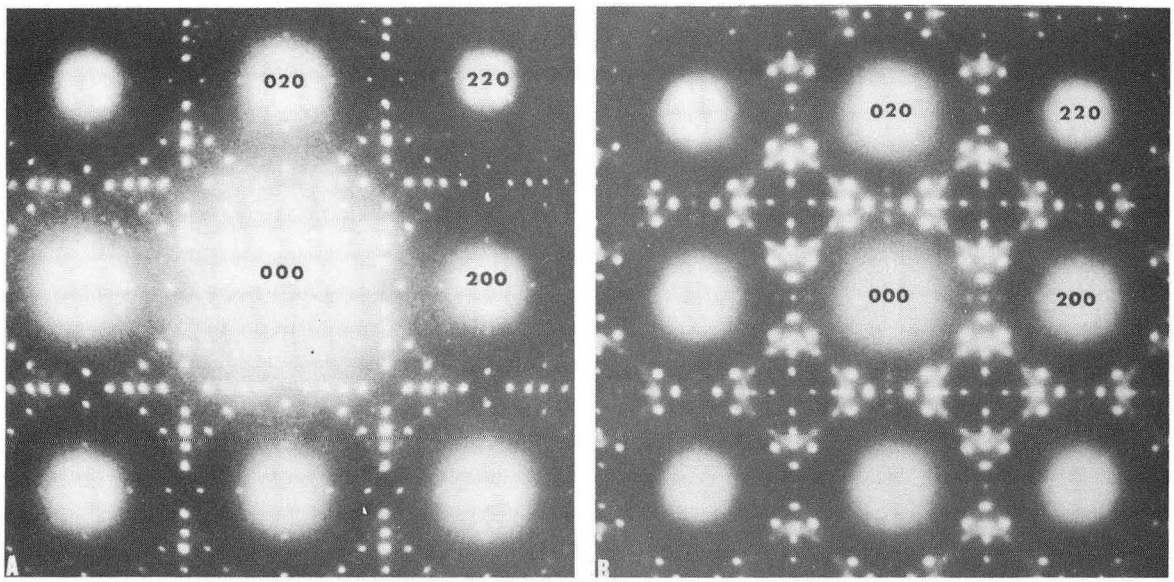

XBB 717-3414A

Fig. 14

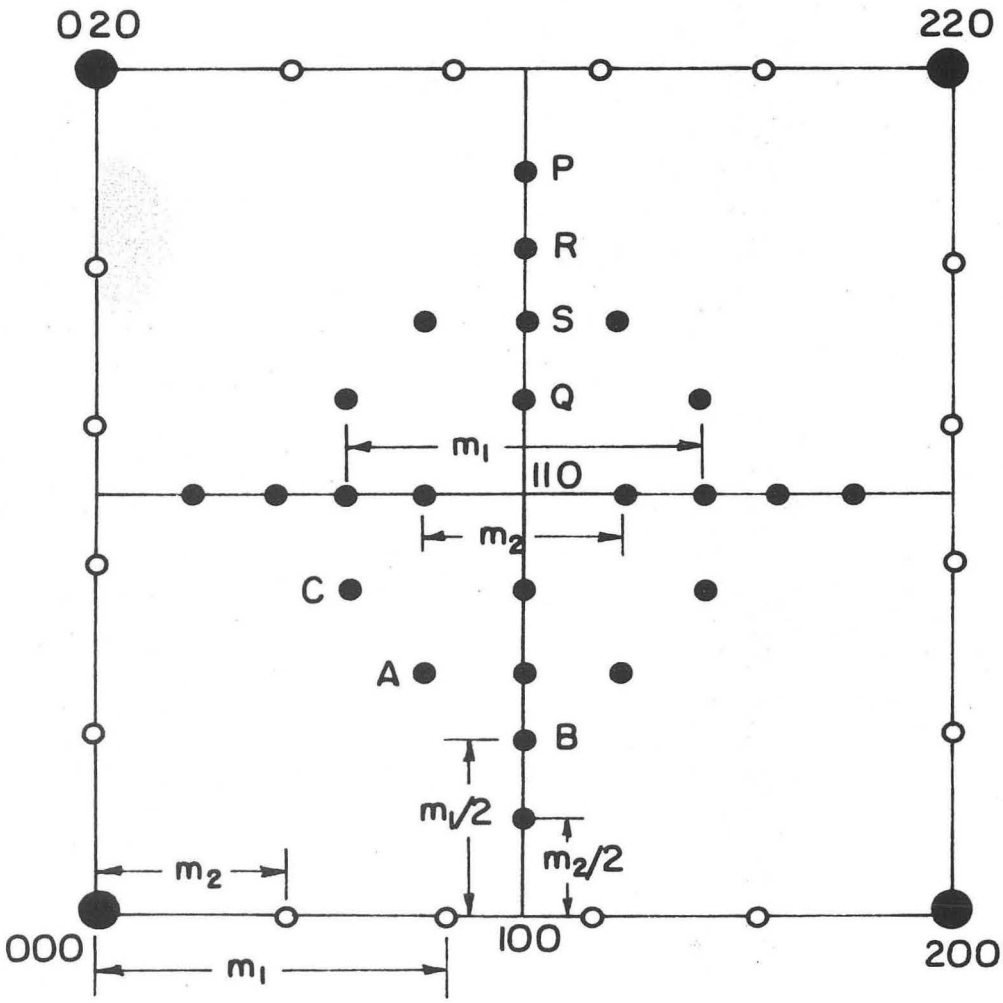
020
220
P
R
S
Q
m_1
110
m_2
C
A
B
$m_1/2$
$m_2/2$
m_2
000
100
200
m_1
FUNDAMENTAL FCC SPOTS
SUPERLATTICE SPOTS
SATELLITES
XBL 717-7008

Fig. 14 (cont.)

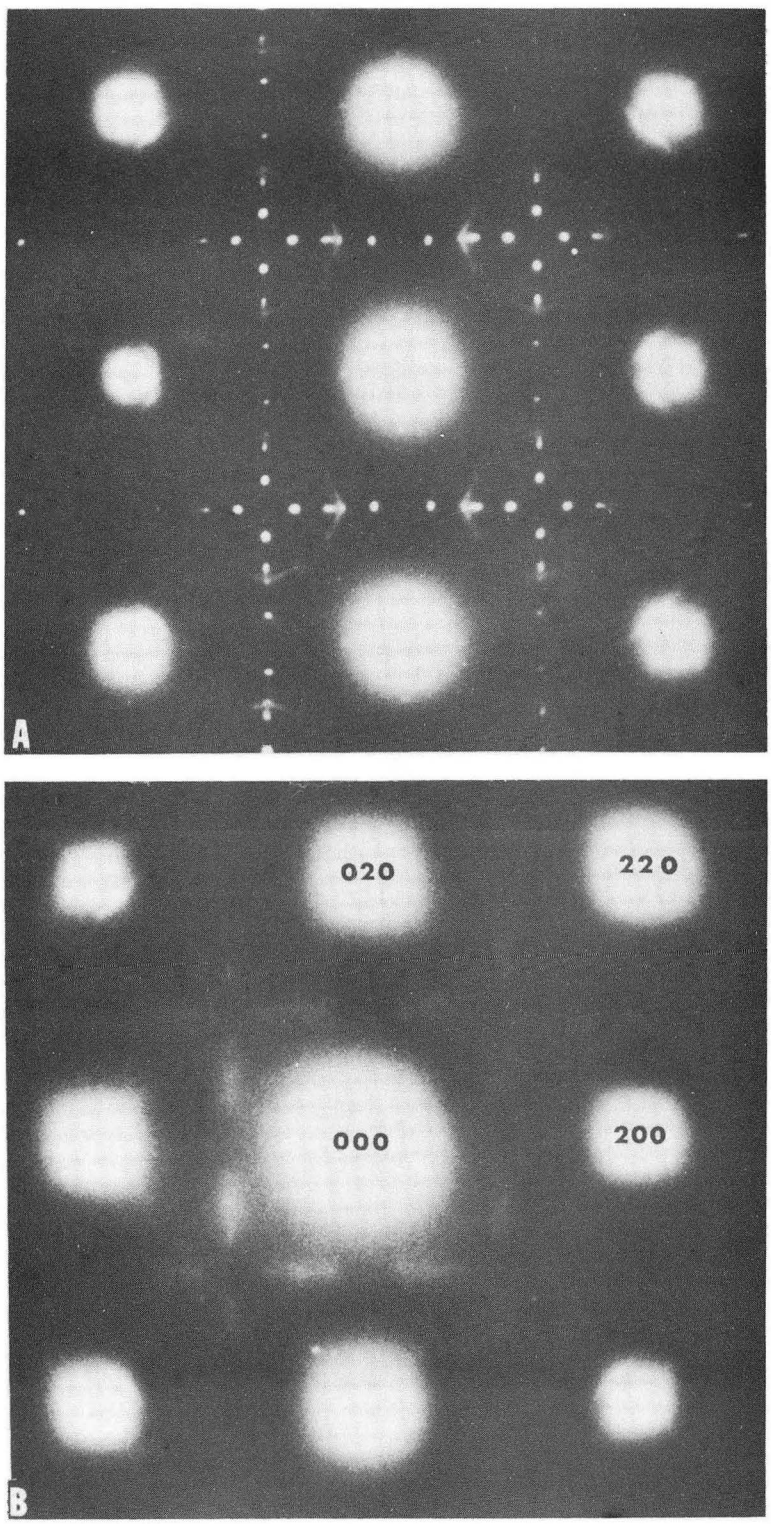

XBB 7110-4762A

Fig. 15

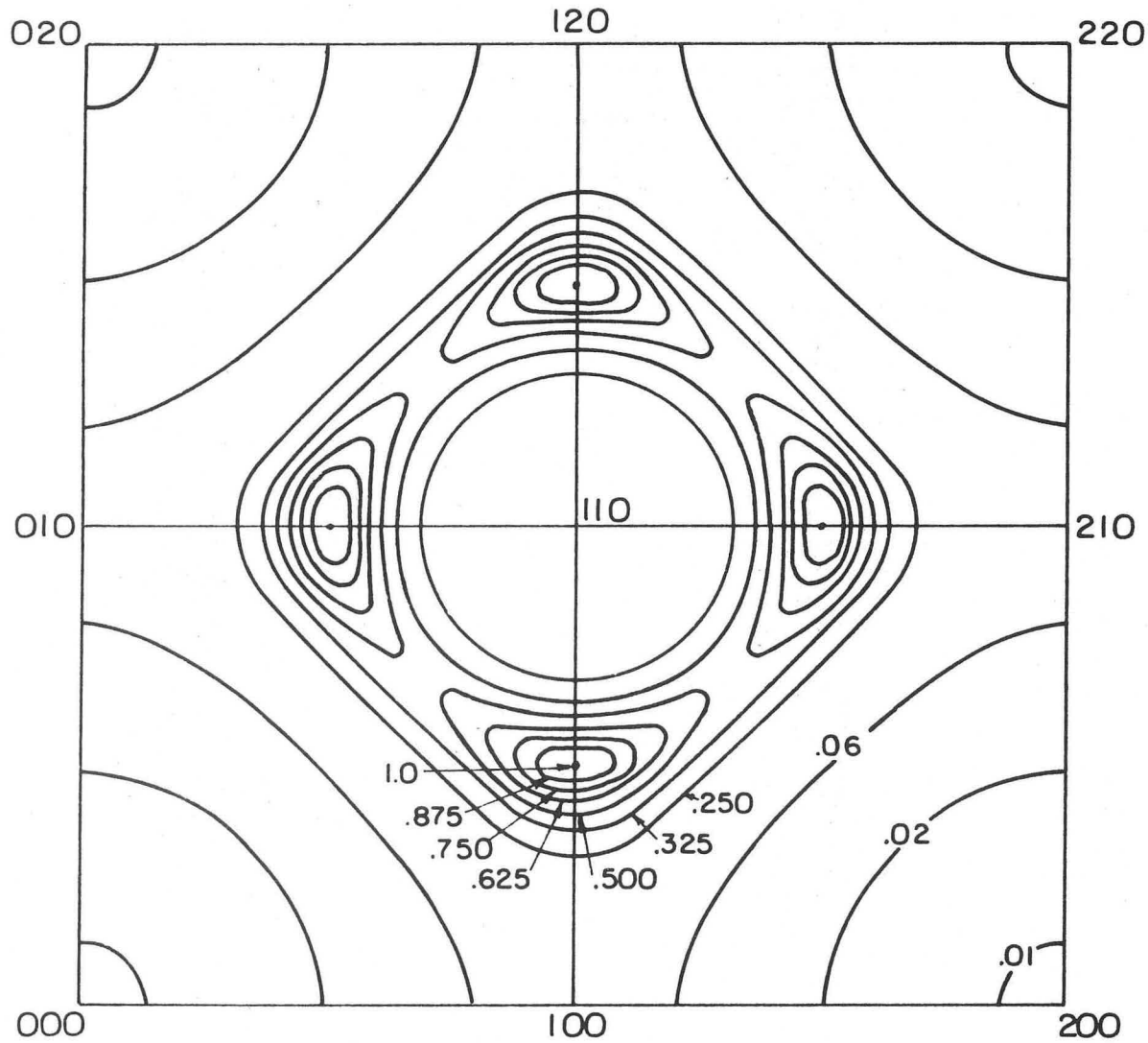

$T_c/T = 0.95$; $V_2/V_1 = 0.4$; $V_3/V_1 = 0.00$

XBL 717- 7007

Fig. 16

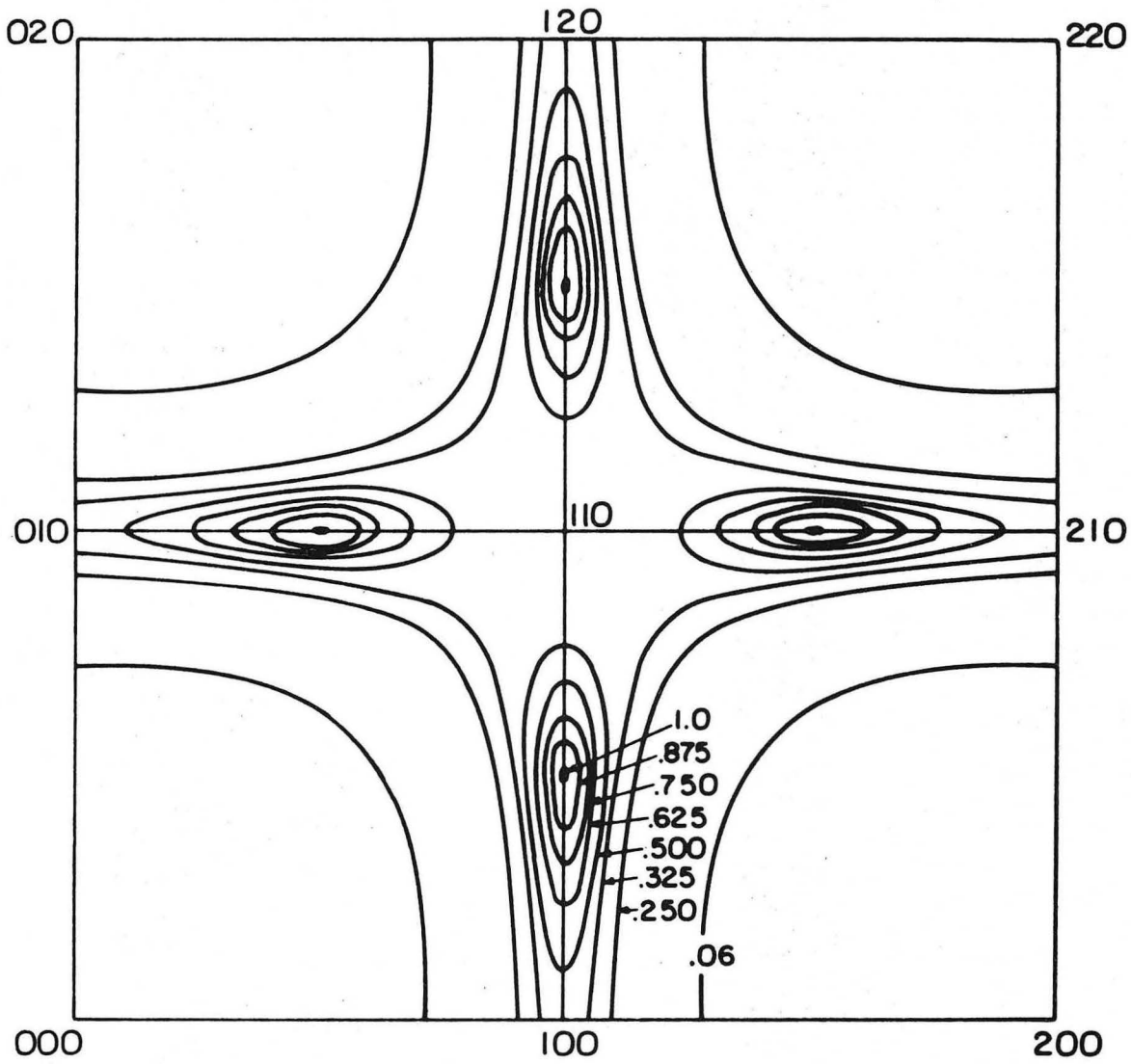

$T_c/T = 0.95$; $V_2/V_1 = -0.7$; $V_3/V_1 = -0.2$

XBL717-7010

Fig. 17

TECHNICAL INFORMATION DIVISION
LAWRENCE BERKELEY LABORATORY
UNIVERSITY OF CALIFORNIA
BERKELEY, CALIFORNIA 94720